The Universe in X-rays: telescopes, observations and theory

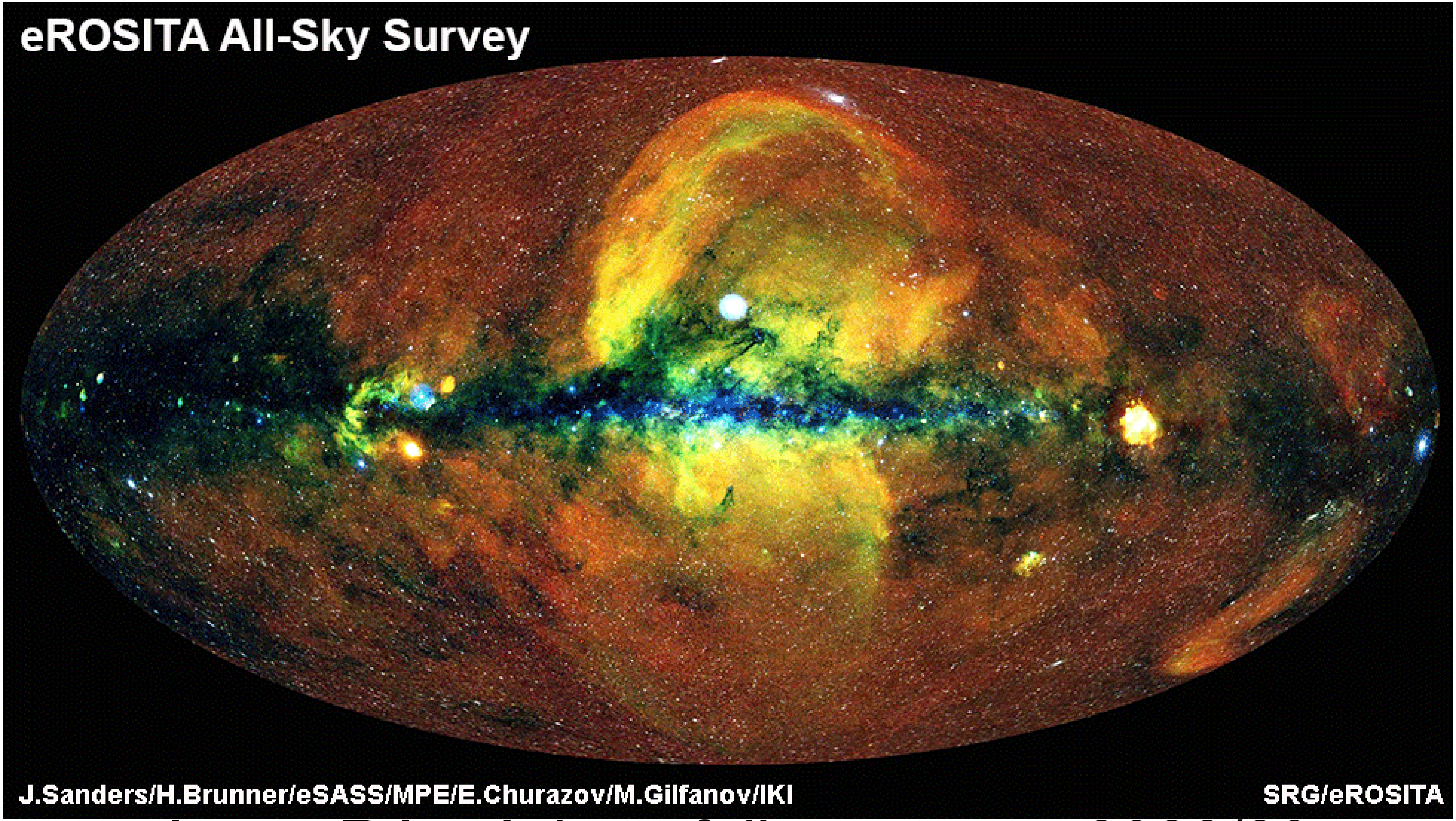

Agata Różańska,   fall semester, 2022/23

By Tahir Yaqoob:

THE INSTRUMENTS OF X-RAY & γ-RAY ASTRONOMY

A few important things to realise:

* To understand observational results it is essential to understand the instrument that was used to obtain the result — far more so than in other wavebands

* Astrophysical sources emit less & less photons at higher energies. X-ray & photon fluxes are small (smaller for γ-rays).
  We need photons, photons, photons
  The best spatial, energy & temporal resolution is useless if we don't have enough photons.

* Non-source signal (background of various kinds) can be comparable to or higher than the signal from the source. Background subtraction very important for most detectors.

⇒ * Therefore observations are limited by photon statistics and/or background systematics.

Lecture 1: PC, GSPC, and SCPC – detectors work in photon counting mode.

Quantum Efficiency:

$$Q = T e^{-d\kappa_w}\left(1 - e^{-h\kappa_g}\right)$$

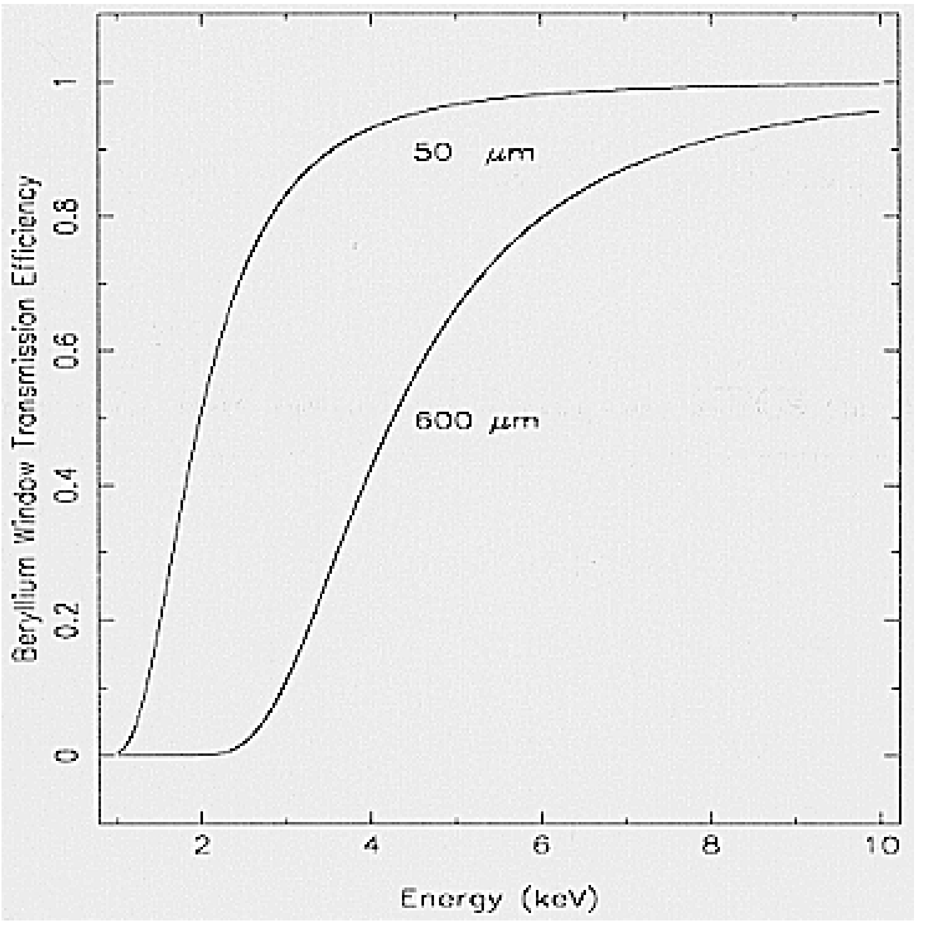

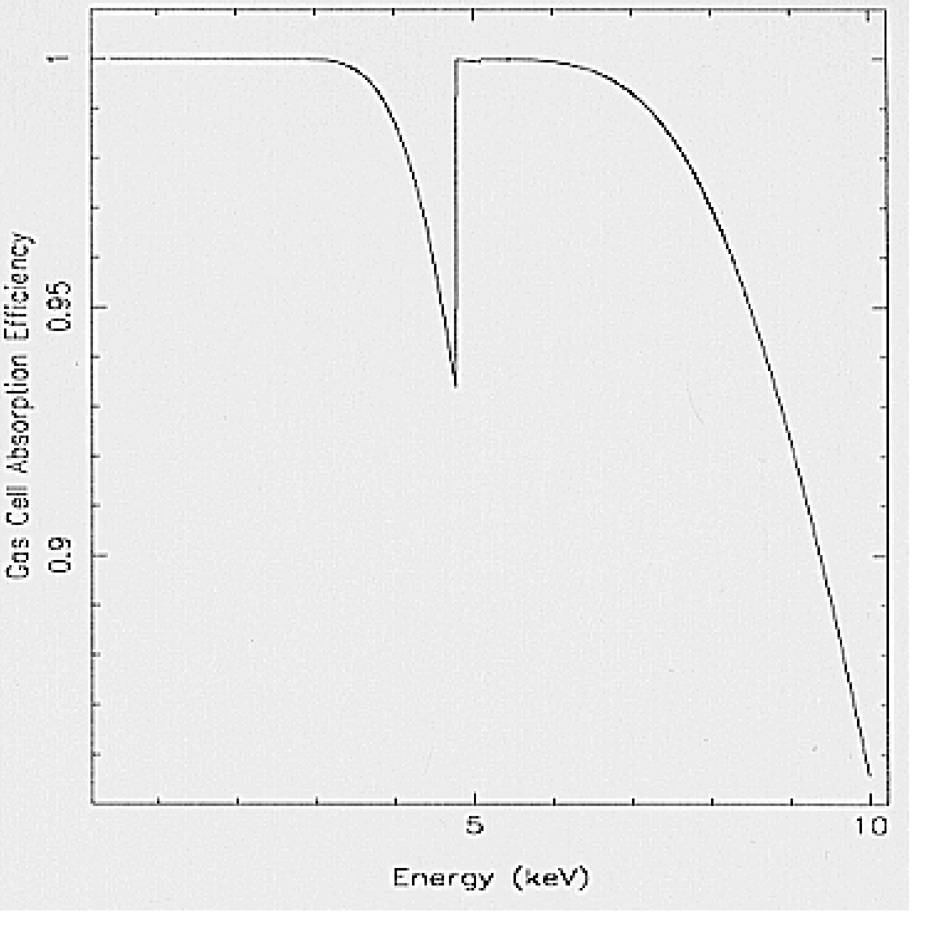

limits the energy range: 2-10 keV

Energy Resolution:

$$\left(\frac{\sigma_E}{E}\right)^2 = \left(\frac{\sigma_N}{N}\right)^2 + \frac{1}{N}\left(\frac{\sigma_A}{\bar{A}}\right)^2; \qquad \frac{\sigma_E}{E} = \sqrt{\frac{F+b}{N}}$$

the background rate exceeds by far the X-ray event rate for the majority of cosmic X-ray sources....

Sophisticated event selected logic is mandatory.....

anticoincidence material

Important definitions:

1 Crab – astrophotometrical unit,
Intensity (mean or flux)
of the Crab Nebula in the range 2-10 keV,

$$1 \text{ Crab} = 2.4 \times 10^{-8} \ \text{erg/cm}^2\text{/s} = 15 \ \text{keV/cm}^2\text{/s}$$

STAR TRACKER – each satellite carries a small optical telescope, which takes pictures of the sky. Those pictures are cross-correlated with optical catalogues, to know where the spacecraft is pointing ..... :)

Point Spread Function, PSF:

- For the source at infinity & a perfect mirror the image should be a point.
- For the X-ray source at infinity & real telescope the image will have finite, bigger than point, size.

- 2 D PSF – the precise shape of the distribution of photon number as a function of position,
  S_{image} < PSF not seen !!!

- As X-ray source gets closer, an image will become bigger than PSF, we can start to measure the spatial distribution of the source.
  When this happens, the source is resolved :)

PSF depends on
Energy and off axis angle.

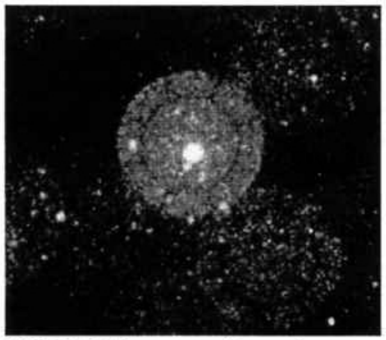
ROSAT image of a point source

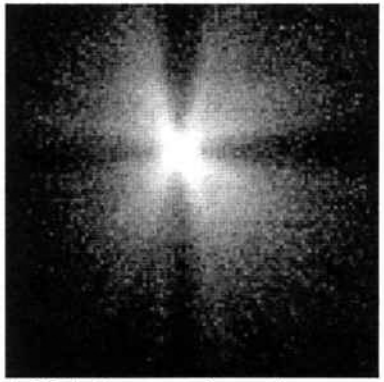
ASCA image of a point source

EEF – Encircled Energy Function;
cumulated energy
contained
within a circle
centered on source,
as a function of radius

ASCA

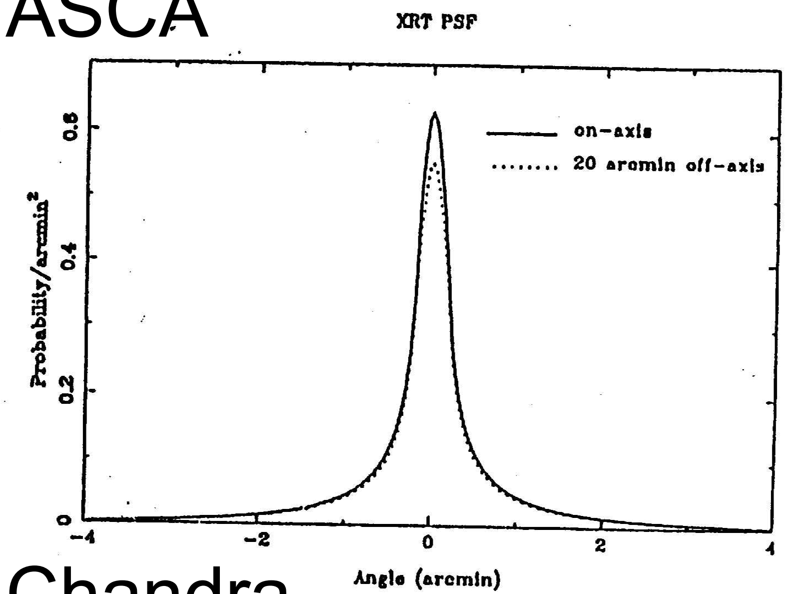

Chandra

(angle from source center)

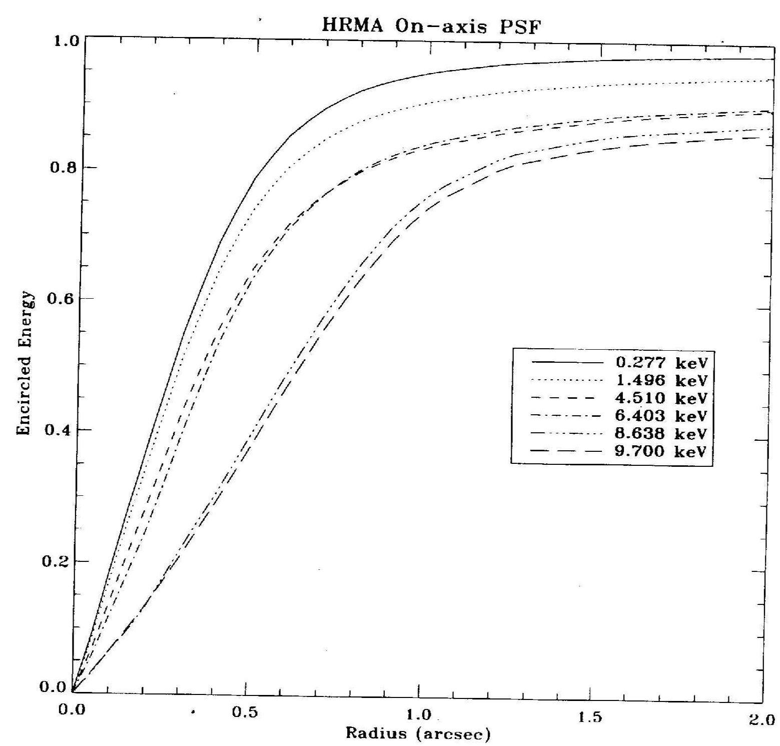

1st Detectors:

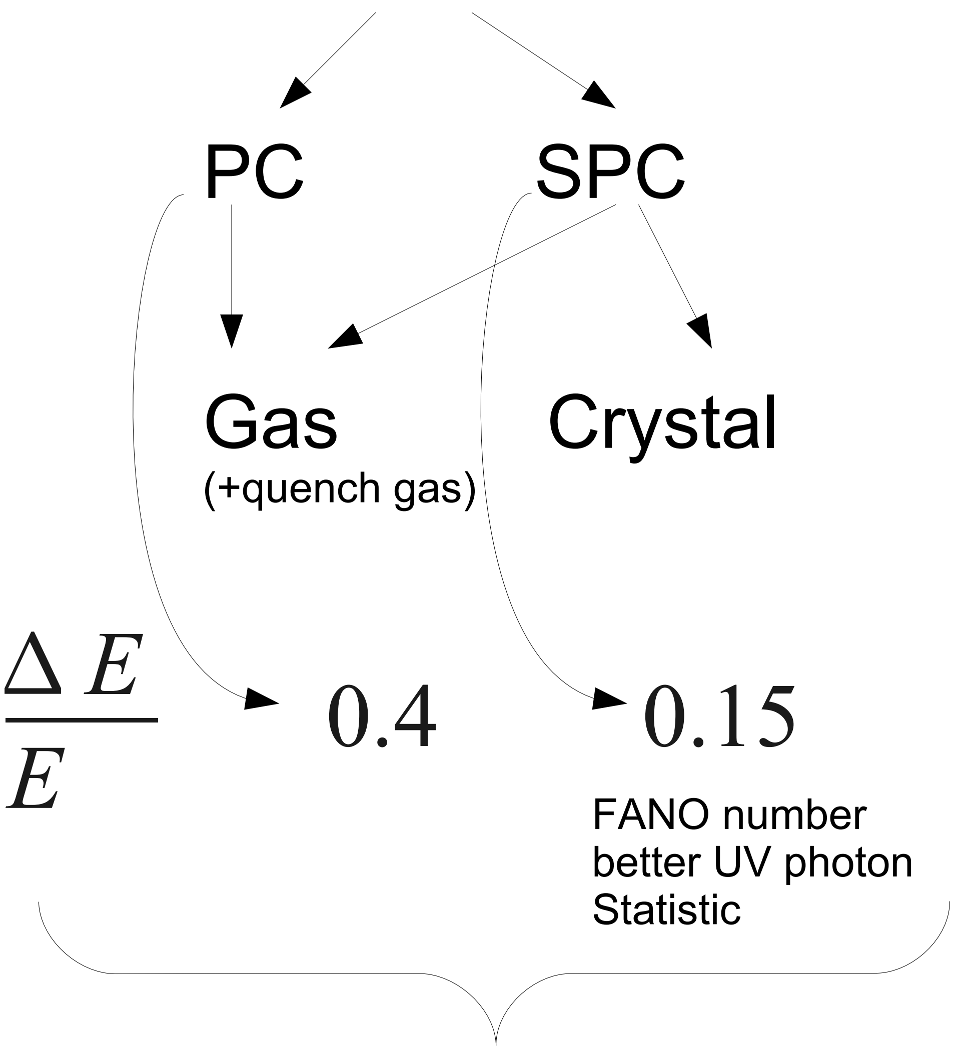

Each photon is like the event in the detector, no information about image.

Bkgr. rejection, time res., det. liftime.

Collimator, anticoincidence system.

Lecture 2: Imaging detectors

Since Wolter's optic is valid up to $\sim$ 10 keV (second part of this lecture)

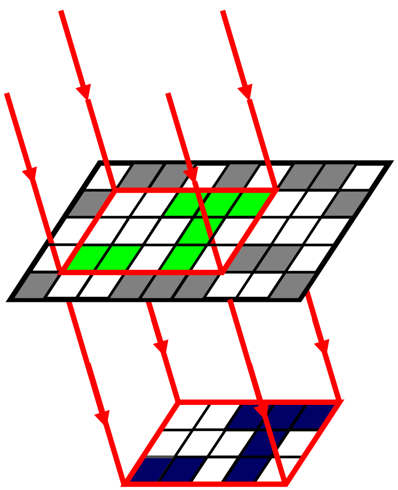

$$A_{eff} = A_{\det}$$

POSITION SENSITIVE DETECTORS were developed to increase spatial and angular resolution.

EINSTEIN, ROSAT, EXOSAT, INTEGRAL.

ON/OFF observations:

This method is not connected to the problem of “imaging”. Knowing the position of the source, the series of observations can be made in two modes:

- “ON” – directly on the source,
- “OFF” – source is outside the collimator response.

Few minutes of integration time each – short time gives almost constant bkgr.
Flux and spectrum is found due to differences between “ON” and “OFF” modes.
HEXTE on RXTE, sensitivity by minimum detectable flux:

$$S_{min}[cts/cm^2/s] = k\left(\frac{2B[cts/cm^2/s]}{T[s]F[cm^2]}\right)^{1/2}$$

Number of standard deviations, by which source is required to be detected above bkgr.

Multiwire PC for X-ray astronomy, IPC (imaging PC), position readout method:

- wire grids of the two cathode are oriented orthogonal to each other to get both coordinates, “rise time” of the signal in both cathode gives both coordinates.

IPC on EINSTEIN $\sim$1mm FWHM.

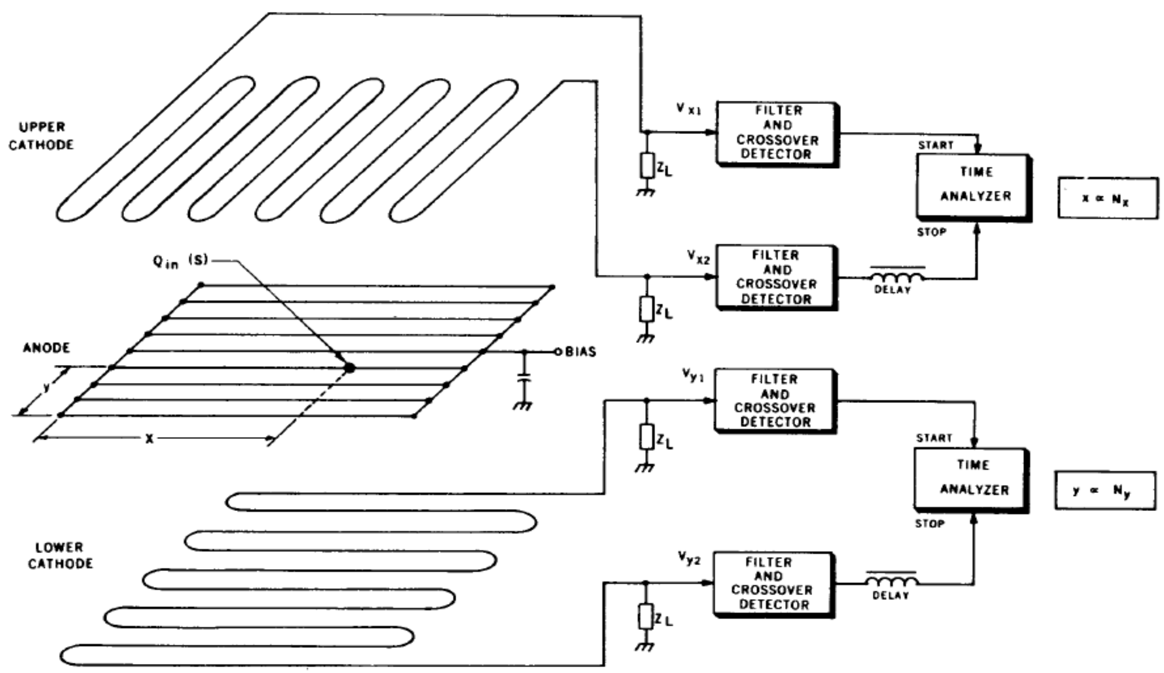

Background X-ray source

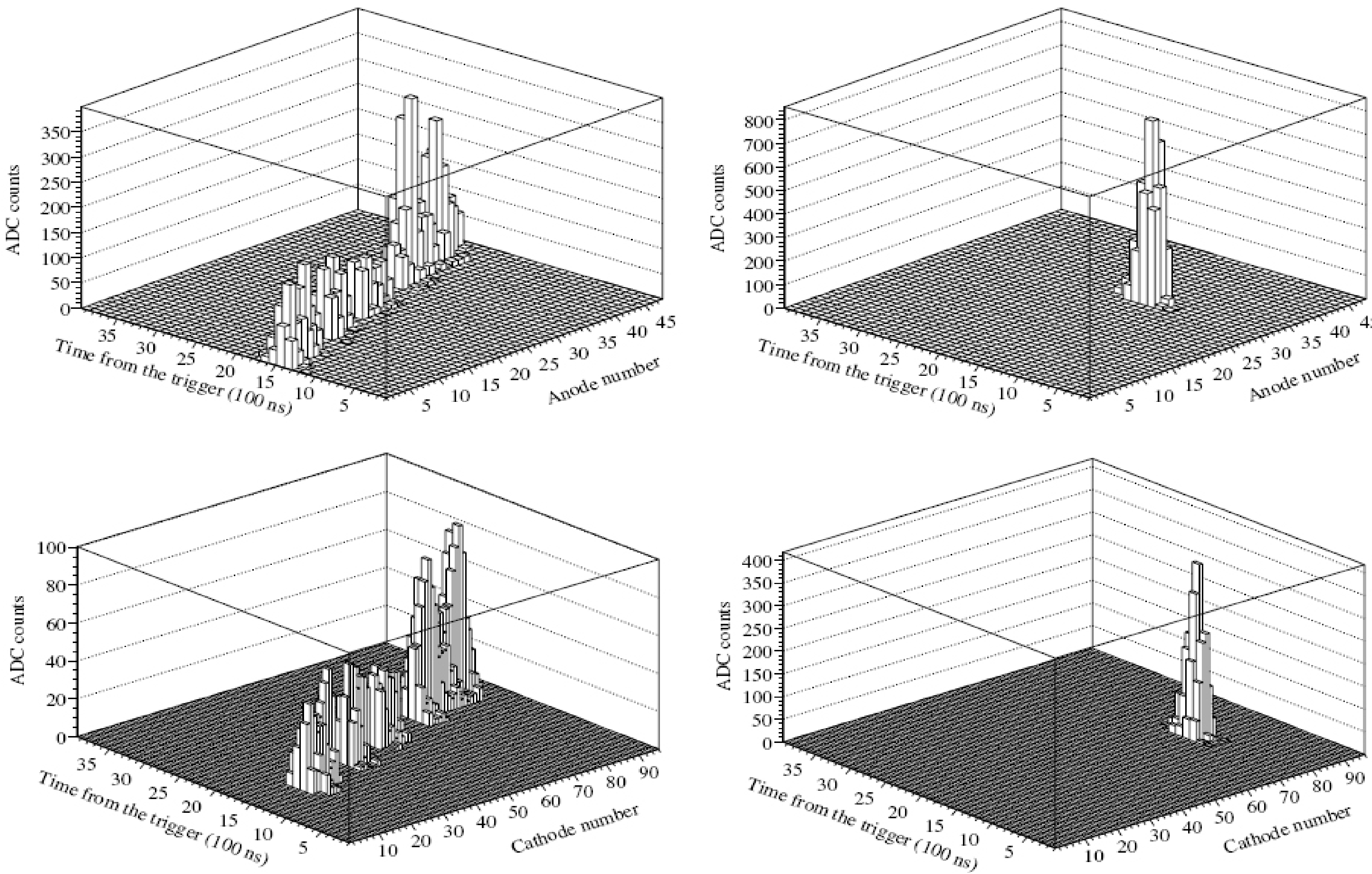

- Measure charge signals induced on the individual strips, charge distribution in cathode strips is twice wider than the distance between anode and cathode, therfore 2-5 strips gives the detection.

ROSAT PSPC $\sim$250 μm FWHM at 0.93 keV

FOV $\sim$2' spacial resolution $\sim$ 2 arcsec

One of the most successful imaging X-ray detectors,
- high mechanical accuracy of the wire grids,
- the detector grain was uniform within 3% over the sensitive area
- 5 side anticoincident counter system and selection logic based on the cathode pattern gives

99.8% of bkgr rejection

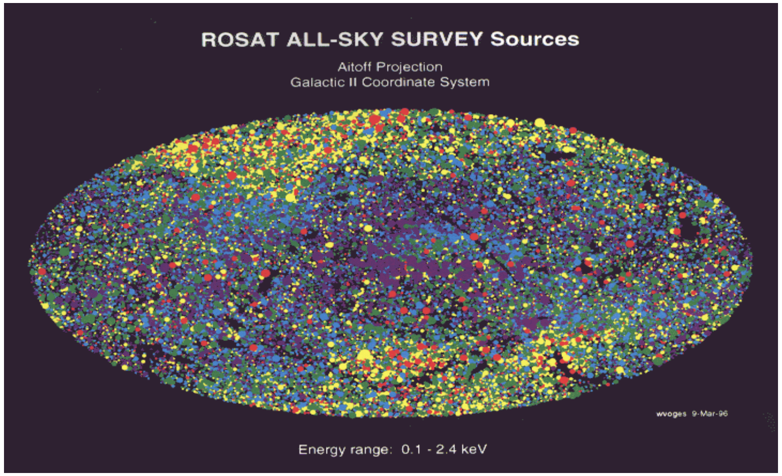

- INTEGRAL JEM-X, The PSPC in the coded aperture mask is a microstrip gas chamber. Instead of wire grid, this detector uses conductive micro structures on a partially isolating glass substrate.

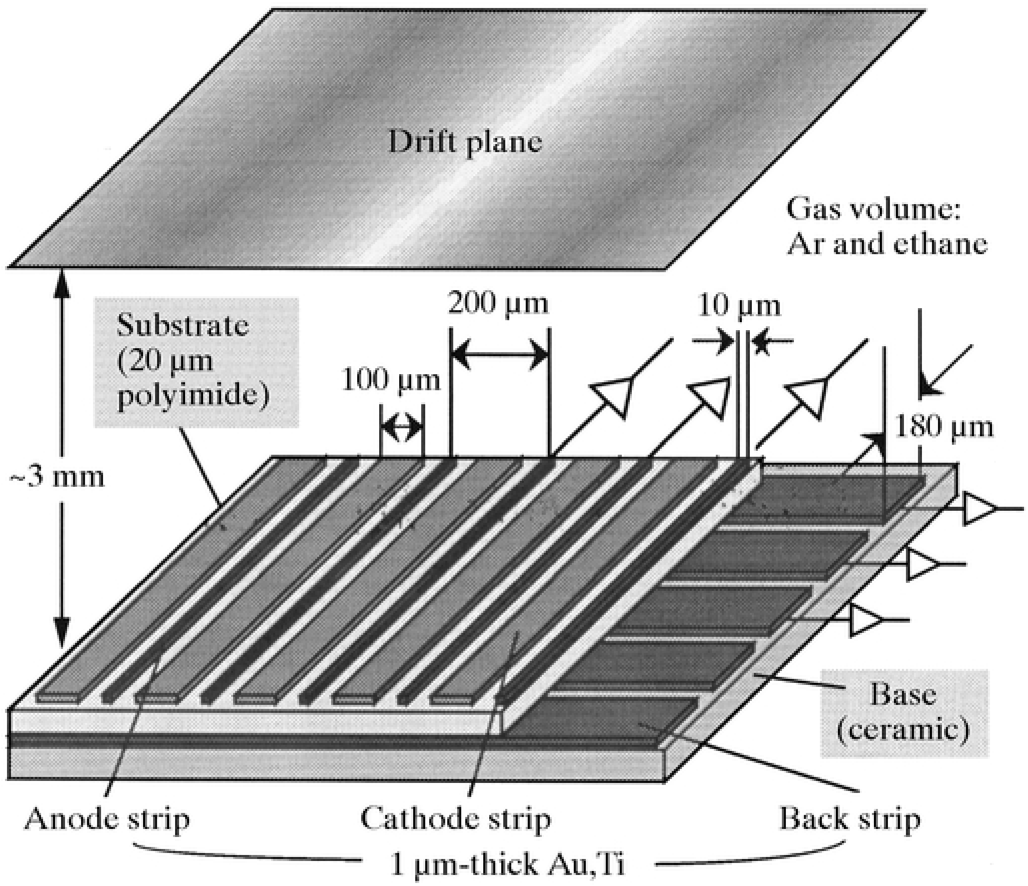

During first week of Operation one anode per day was lost – discharges triggered by heavy ionizing events.
Lowering the gain by a factor of 3, the Radiation damage was Reduced to a level:

- one anode strip per 2 months..... :(

Aperture modulation telescopes (temporal or spatial):

Indirect imaging capability is achieved due to placing a mechanical, X-ray absorbing collimator in front of a flat X-ray detector - “slat collimator” consisting of parallel metallic plates (mask).

Due to sky scanning, the flux of X-ray source will be modulated according to the triangular collimator response function.

Basic principle of imaging due to aperture modulation- “shadow cameras”.

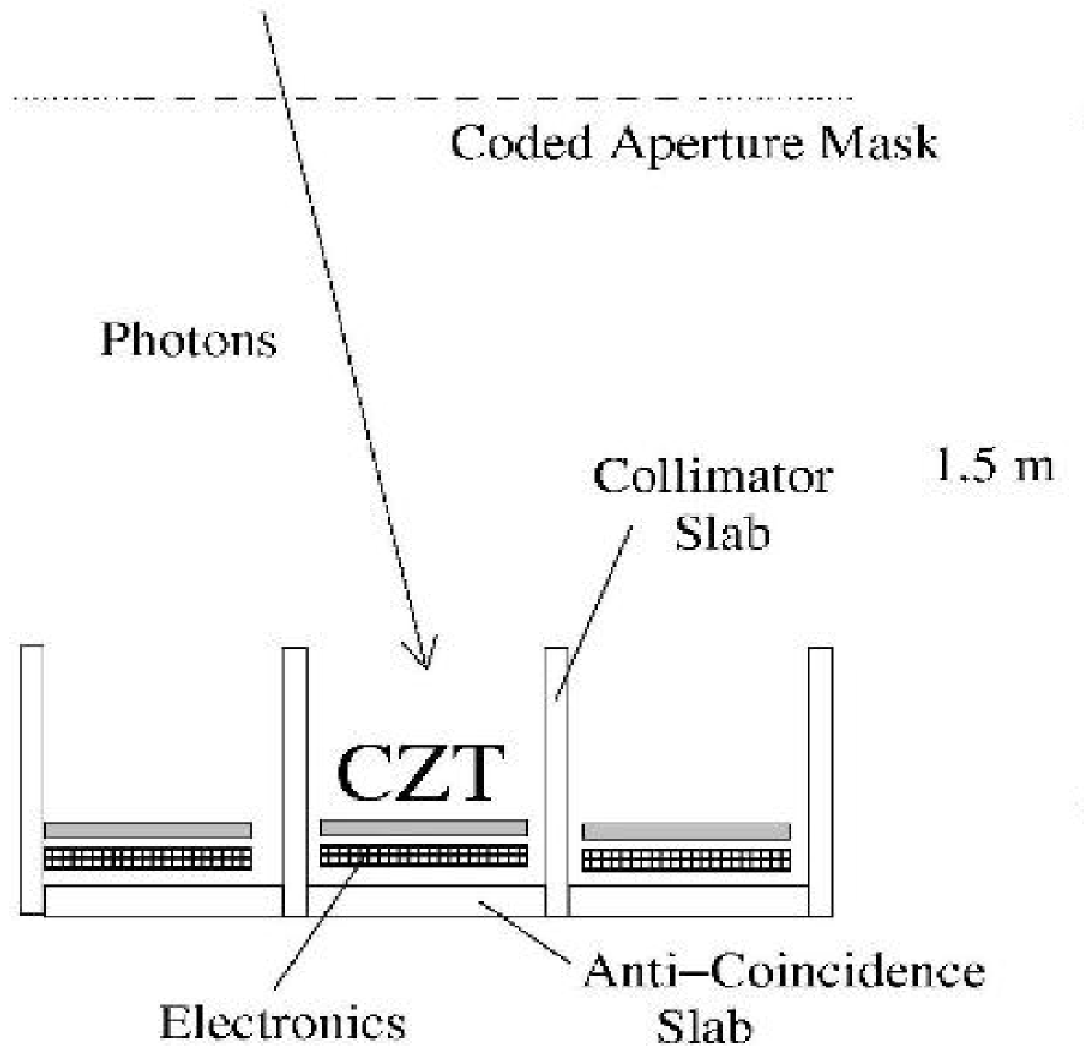

Scanning with “slat collimator”:

Image the sky by “monitoring instruments”. Two scanning measurements are needed in two perpendicular directions.

UHURU - first All Sky Survey in X-rays 1970-72
2 gas PC with metal collimators with:
5° x 10° 2° x 10° FWHM, 339 sources.

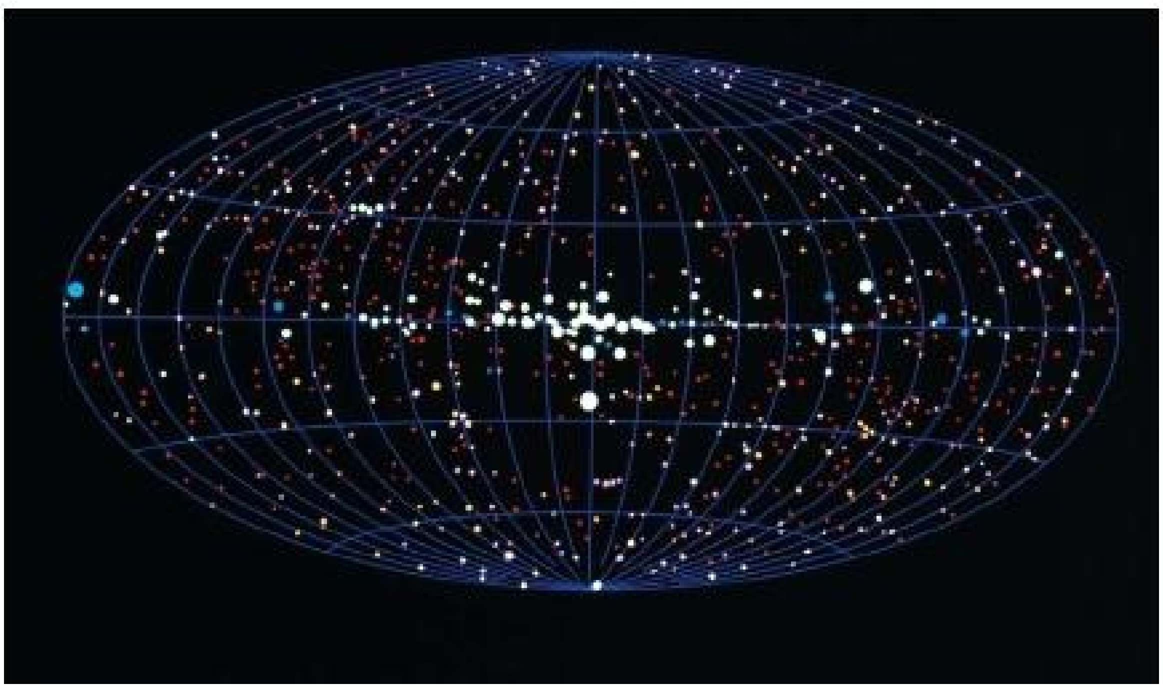

Repeated by HEAO-2, first imaging X-ray telescope.
EINSTEIN, 1978.

Rotational modulation Collimators:

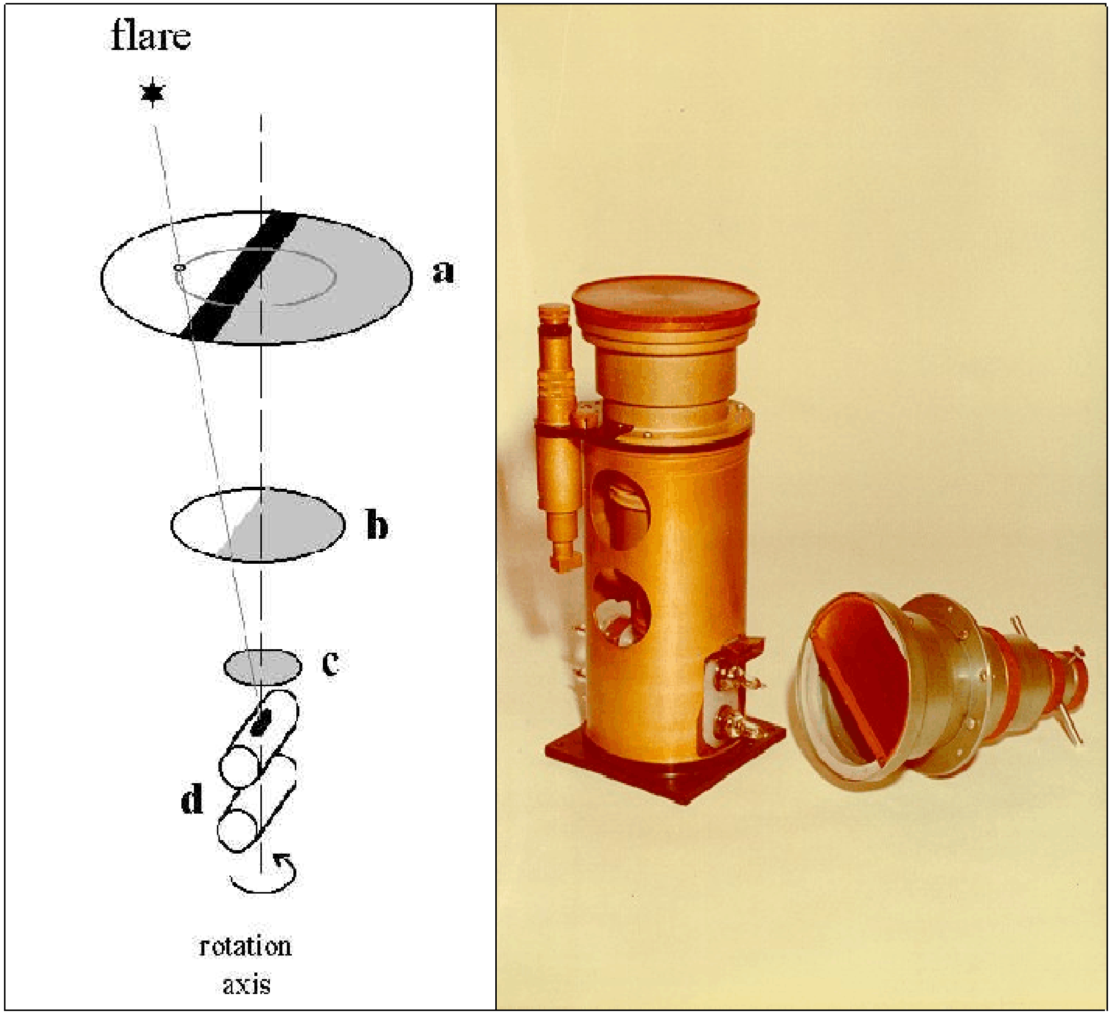

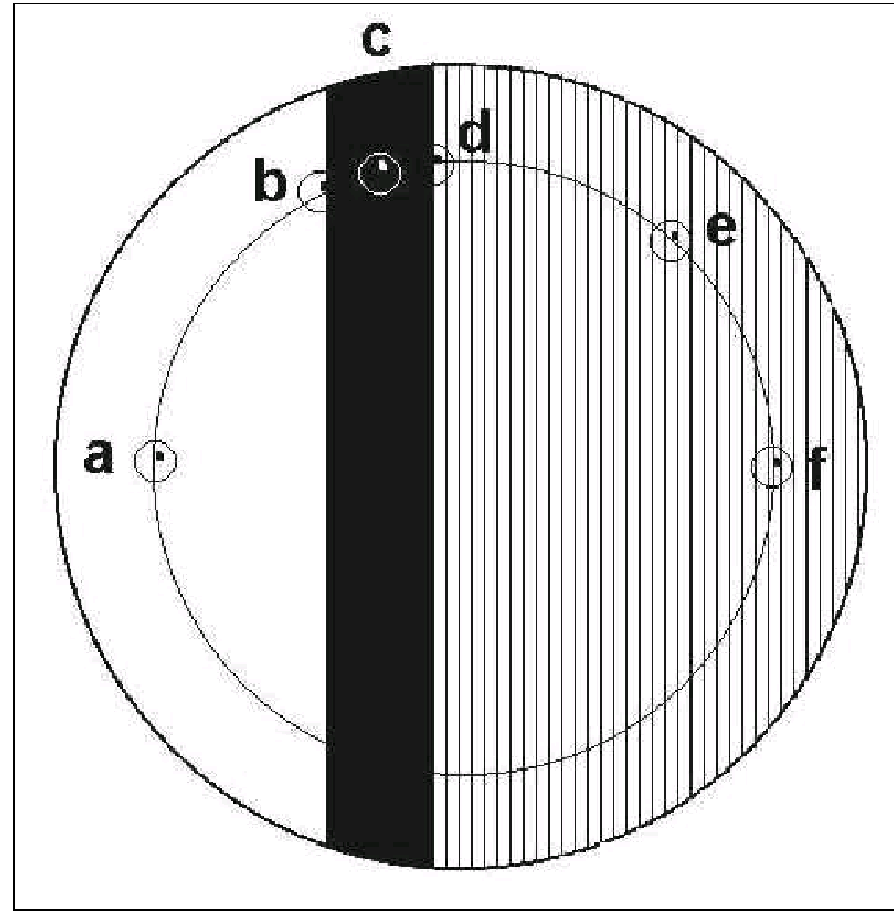

Sylwester + 2000, INTERBALL – Tail Mission
Depending of modulation unique position can be found.

Spatial aperture modulation, masks + 2 D position sensitive detectors.

Dicke 1968 ApJL

Pattern of holes
in absorption plate
gives unique spatial
code- coded mask.

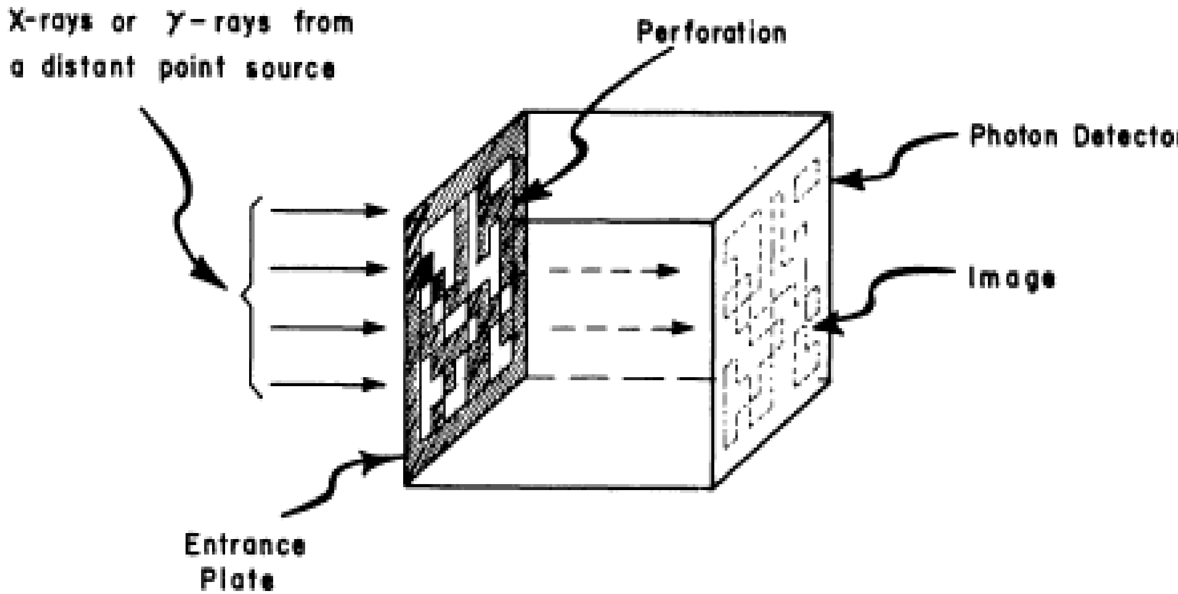

Depending upon the direction of the single point source (at infinity), the image can be characterized by the function $f_1(x) = f(x - x_1)$, where f_1 is to be interpreted as a measure of photon distribution, photographic grain density, probability distribution of sparks in the spark chamber, photoelectron distribution, or the like. The coordinate now refers to coordinates in the image plane, and x_1 characterizes the position of the source. The convolution of f_1 and f is the integral over the image plane

$$g(y) = \int f_1(x) f(x - y) dx = \int f(x - x_1) f(x - y) dx \,. \qquad (1)$$

http://astrophysics.gsfc.nasa.gov/cai/coded_intr.html#section2

Most popular only with half blocked transmission.

Any shift of the pattern on the detector surface is directly related to the shift in source position.

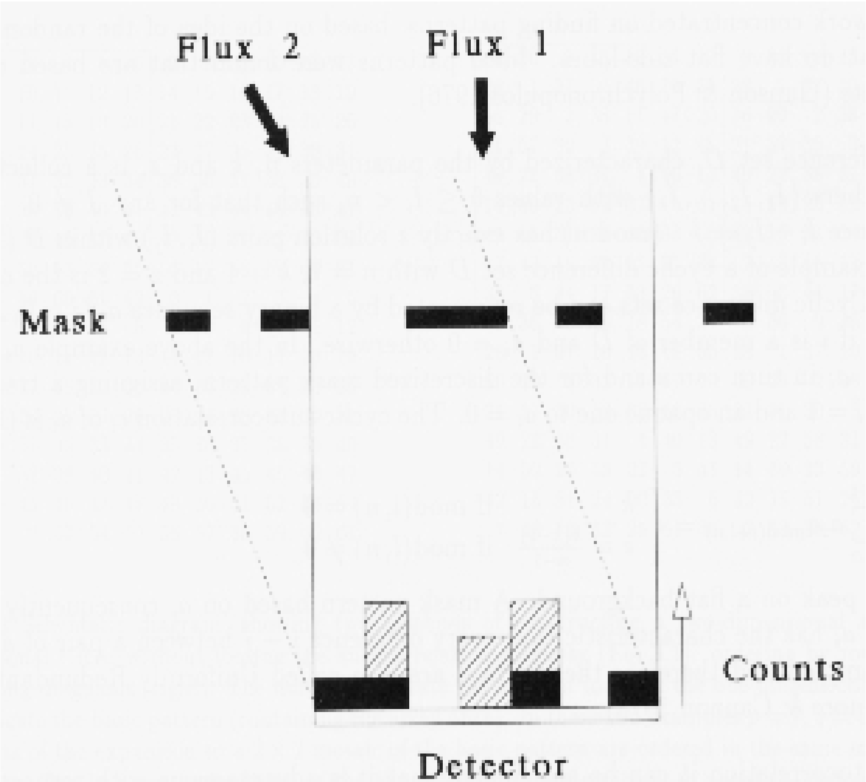

Two point sources illuminate a position-sensitive detector through a mask. The detector thus records two projections of the mask pattern. The shift of each projection encodes the position of the corresponding point source in the sky. The “strength” of each projection encodes the intensity of the point source.

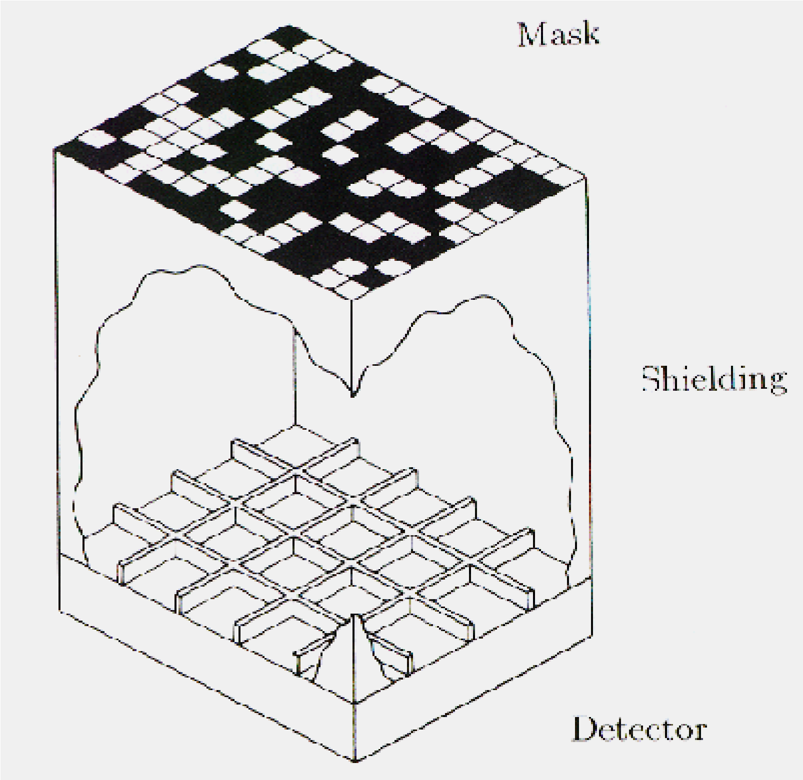

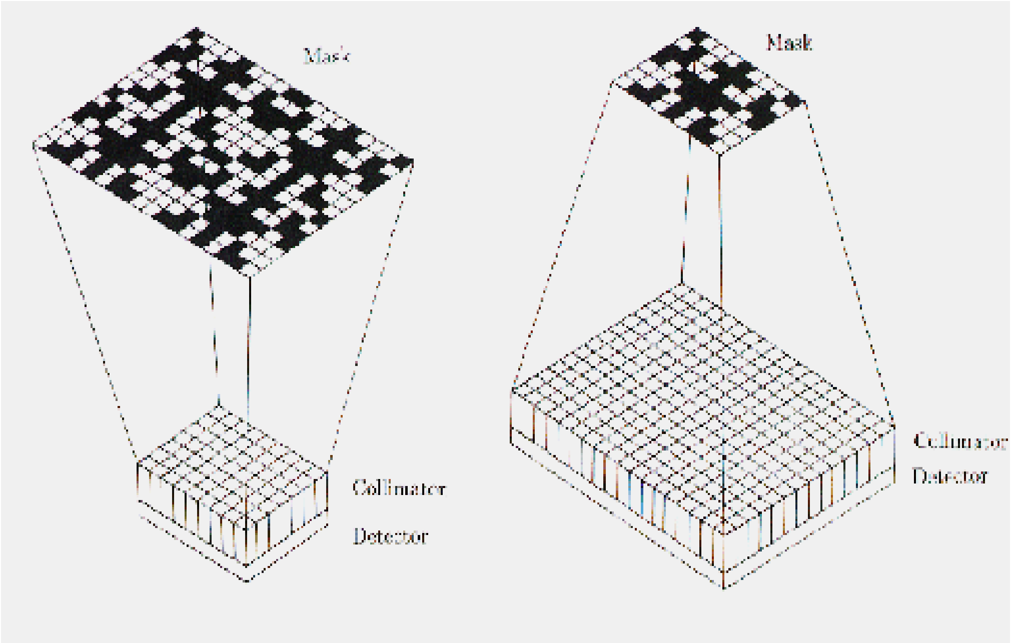

Fully coded field of view – FCFOV – photons from any source reaching the detector must pass through the mask.

Partially coded field of view – PCFOV- boundaries when Fraction of the detector area which is coded reaches zero.

FCFOV < PCFOV

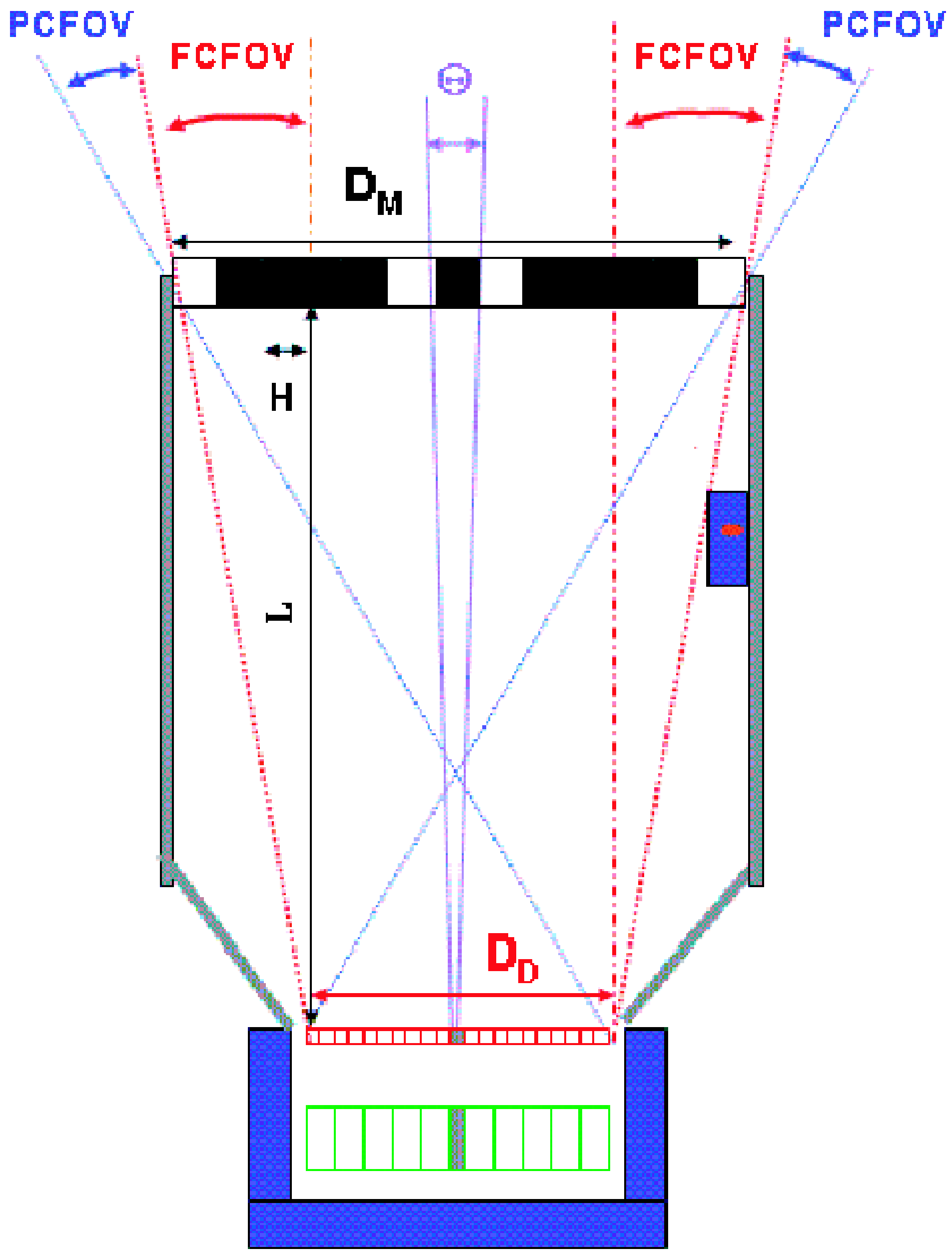

Angular resolution proportional to the d/D,

d- characteristic length scale of the mask pattern (width of the holes),
D- distance between the mask and the detector.

Ang. res. of the order of d , can be better depending on the photon statistic.

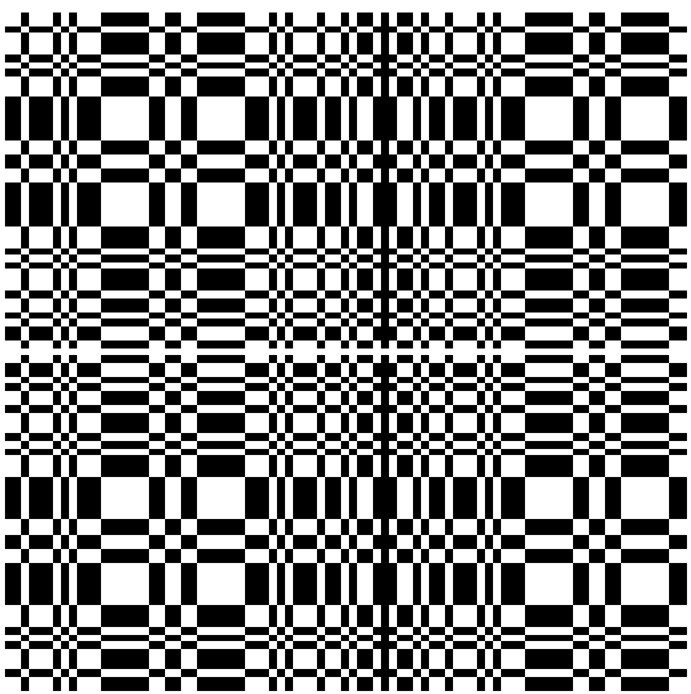

INTEGRAL

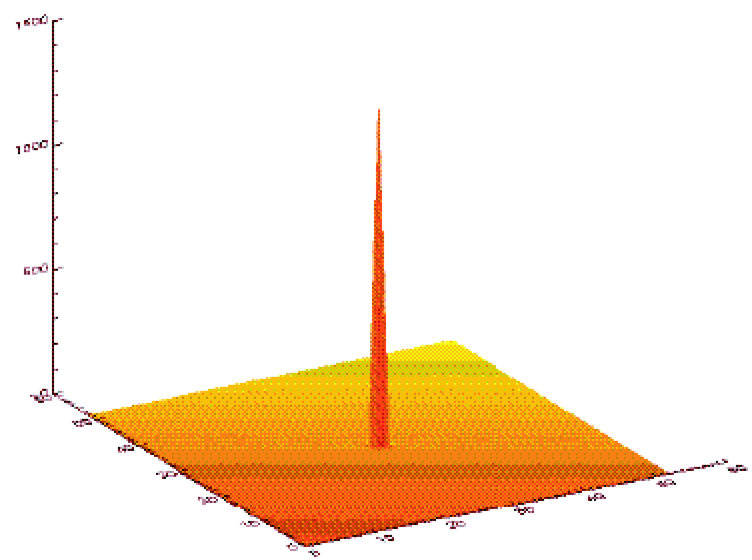

Classical "inverse problem":

2 D array of pixels filled with intensity values,

Observed intensity distribution must be interpreted ("unfolded") using coding function provided by the mask pattern.

Unknown sky distribution is reconstructed from a measurement.

Basic coding equation:

x – vector describing 2D coordinate in the respective plane

$$D(x) = M(x) \times S(x)$$

Observed detector distribution

Aperture modulation function

Sky dsitribution

$$D(x) = M(x) \times S(x)$$

The resulting sky image is not unique, but rather subject to uncertainties that can be quite large.

- uncertainty from counting (Poisson) statistics – generally substantial because of the presence of background.

- S(x) is superposition of the uniform diffuse X-ray bkgr and all existing sources (point like and extended) in the total FOV:

$$D(x) = M(x) \times (B_{sky}(x) + \sum (S_i(x)))$$

- detector bkgr – locally produced secondary potons, Indistinguishable from photon events.

- for sources in PCFOV incomplete coding adds a "coding nise"

Only for special codes, it is possible to invert M(x) directly

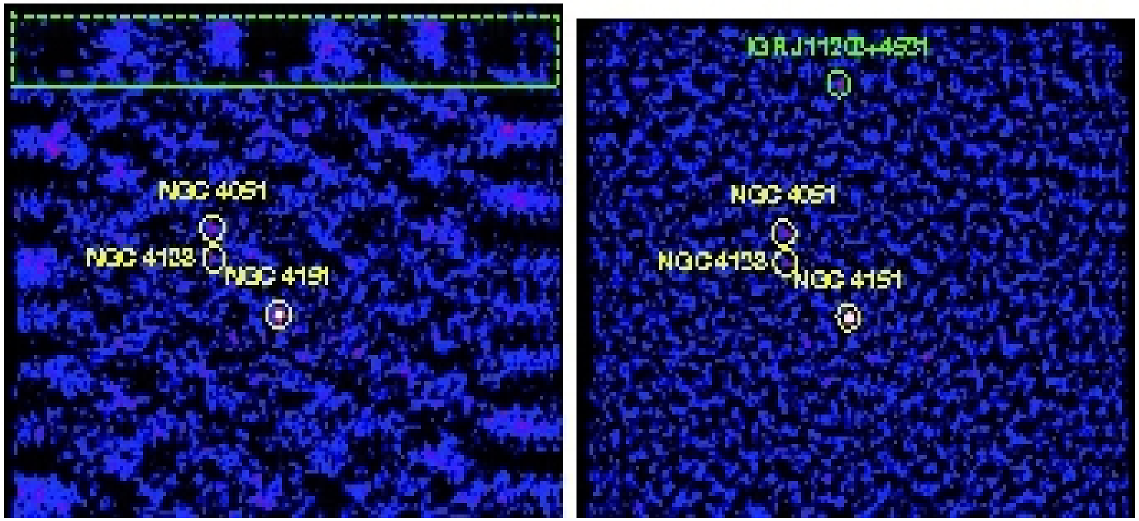

INTEGRAL 20 Msec

Krivonos+ 2010 A&A, 519, A107

IBIS coded mask:

SPI

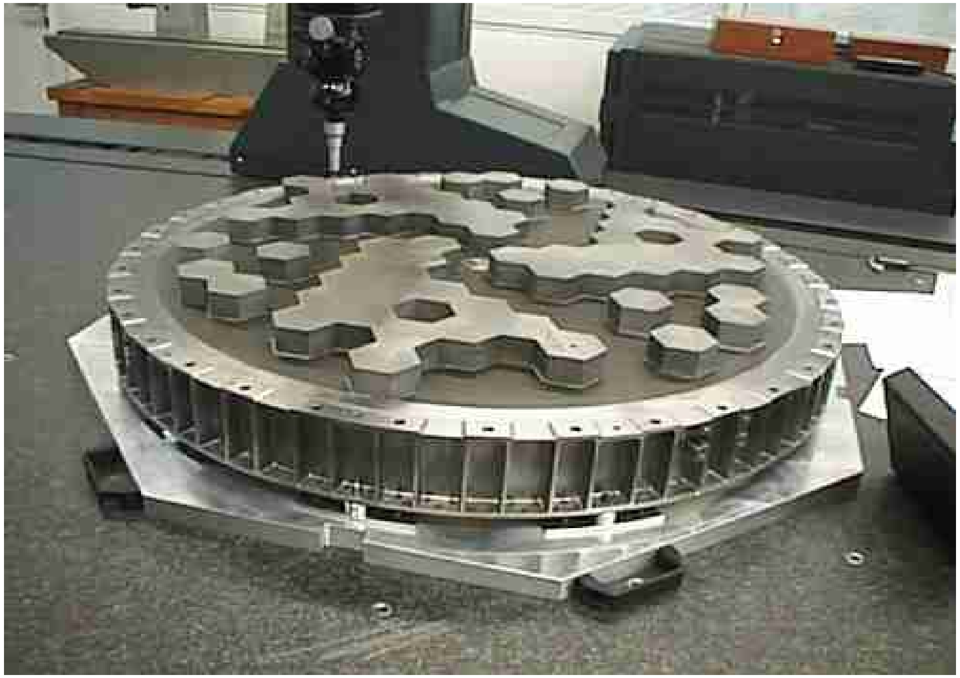

JEM-X

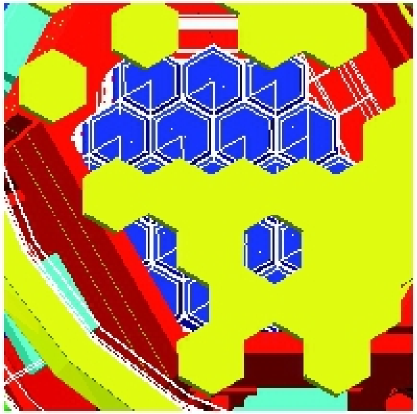

Fig. 3. The coded mask elements (yellow) overlaying the 19 SPI detectors (blue), as viewed from the direction of the incoming GRB photons generated using the simulations. Detectors 14, 15 and 16 (*bottom left*) are partially obscured by the anticoincidence shield.

X-ray Optics (Wolter): Why?

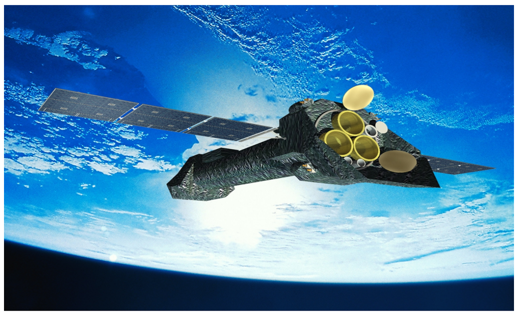

- Best 2D angular resolution
- Distinguish nearby sources
- Use morphology to choose models
- To “gather” weak fluxes of photons
- Simultaneously measure SRC & BKGR
- Best spectral resolution
- Dispersive spectrometers

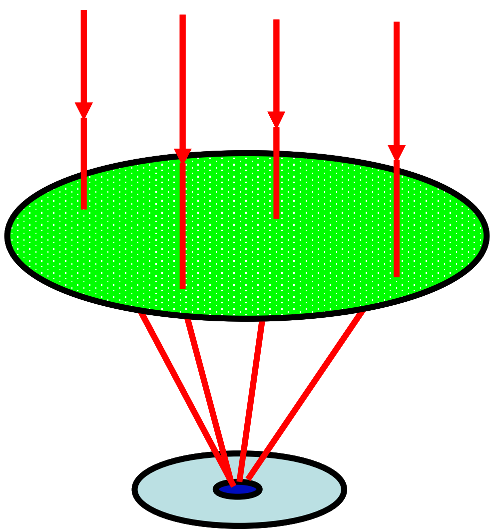

$$A_{eff} >> A_{\rm det}$$

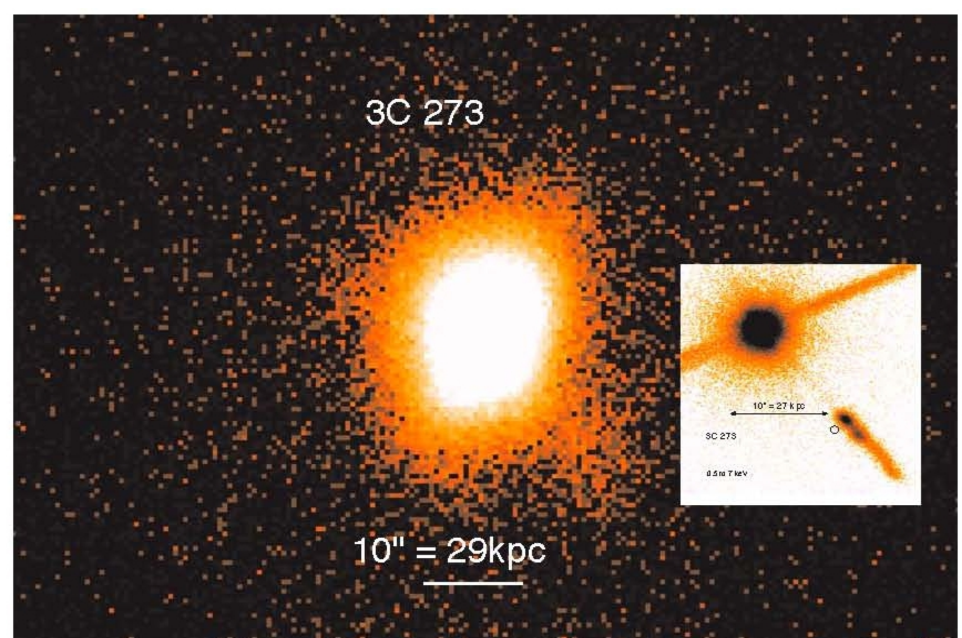

X-ray Optics:

1. X-rays must be reflected:

   a) Total external reflection

   b) Fresnel's Equations

2. X-rays must form an image:

   c) Scattering

   d) Mirror's Figure

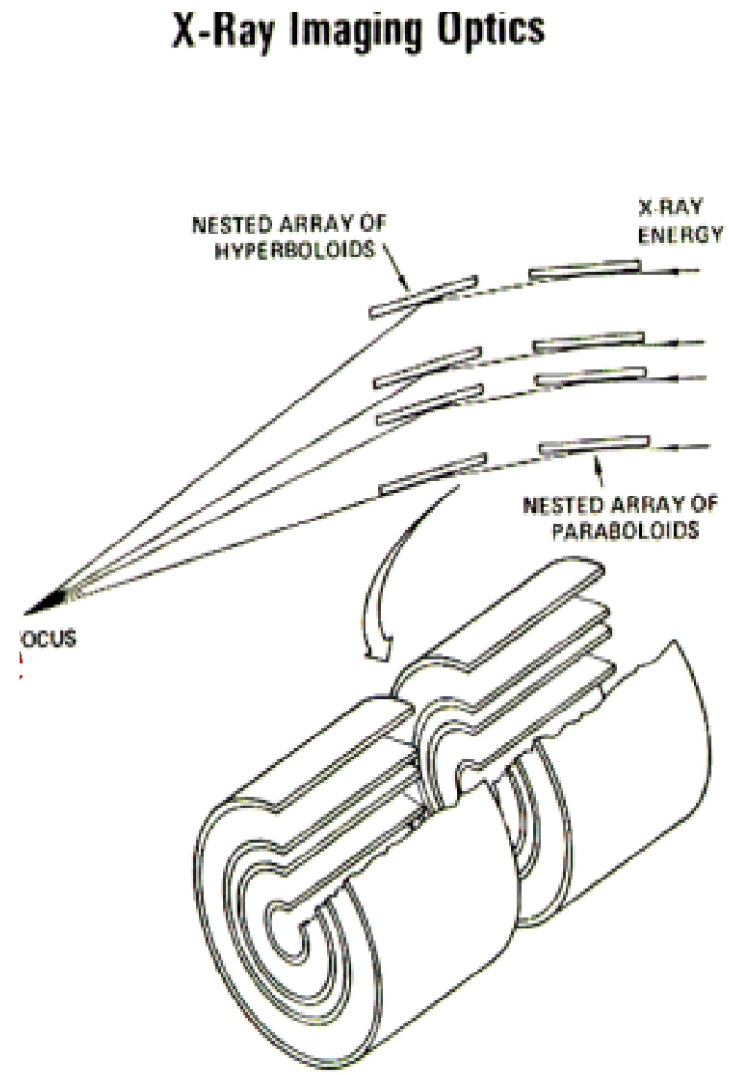

a) Grazing incident reflection for X-rays:

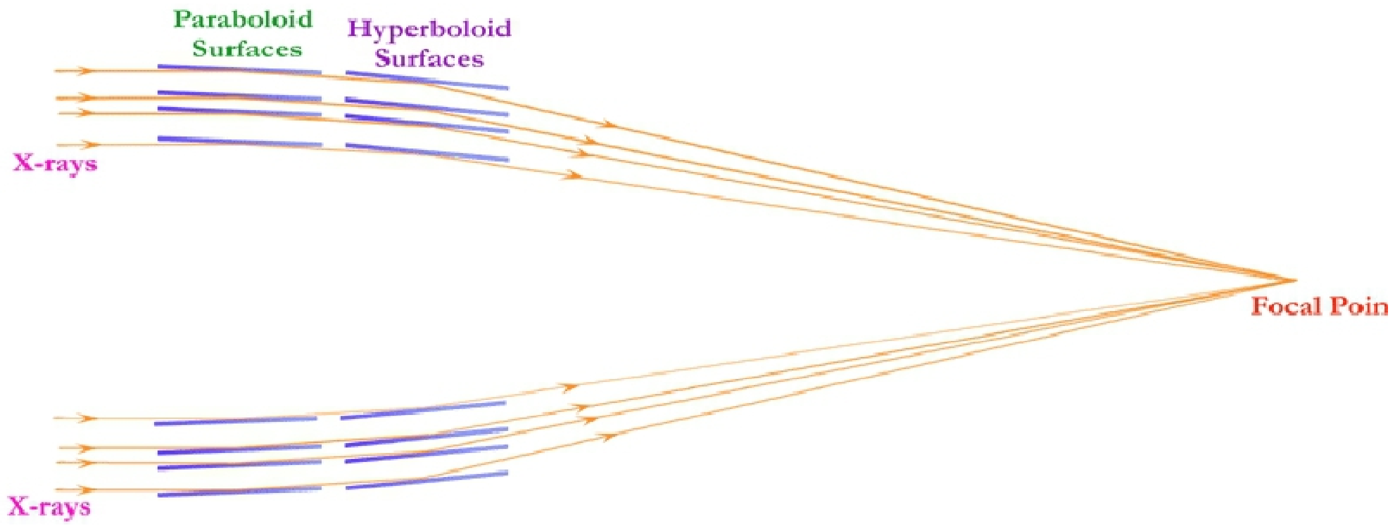

- X-rays reflect at small grazing angles: $\alpha = 90° - \theta$,
- Reflection of any wave by an ensemble of electrons is coherent only in very special directions:
  angle of incidence equals angle of reflection;

$$\theta_i = \theta_r$$

$$\alpha_i = \alpha_r$$

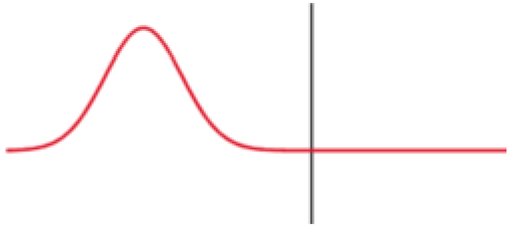

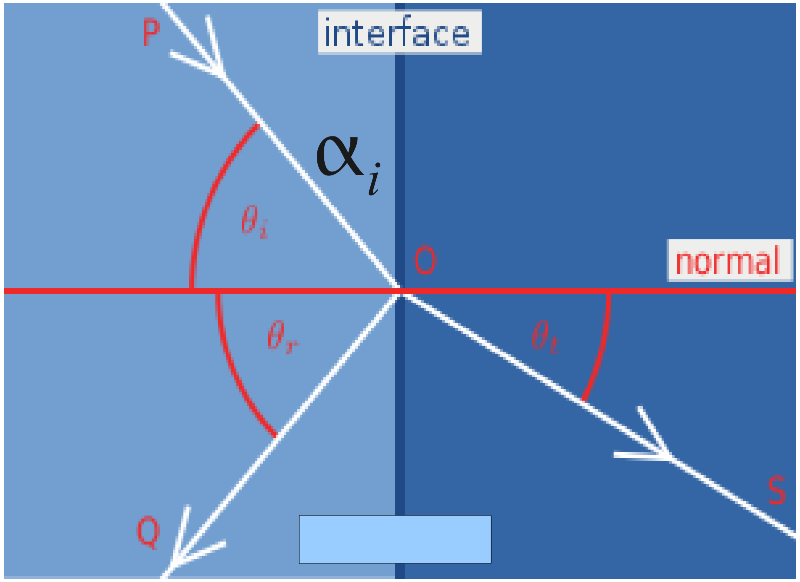

θ_i – incident angle

θ_r – reflected angle

θ_t – refracted angle

α_i – grazing angle from the surface

vacuum:	complex index of refraction
$n=1$	$n=1-\delta-i\beta$

δ, β → optical constants - functions of energy or wavelength of photons.

Refraction index: $n = 1 - \delta - i\beta$

Consider the plane wave:

$$E = E_0 \mathrm{e}^{-i(\omega t + \boldsymbol{kr})}$$

The velocity of wave in the vacuum: $\boldsymbol{c} = \omega / \boldsymbol{k}$

in the material:

$$\boldsymbol{c} / \boldsymbol{n} = \omega / \boldsymbol{k}$$

Substituting **k** and **n** : $E = E_0 \mathrm{e}^{-i[\omega t - (\omega / c)(1 - \delta + i\beta)\boldsymbol{r}]}$

$$E = E_0 \underbrace{\mathrm{e}^{-i\omega(t - \boldsymbol{r}/\boldsymbol{c})}}_{\text{wave in vacuum;}} \underbrace{\mathrm{e}^{-i(\omega\delta/c)\boldsymbol{r}}}_{\text{small phase change; less than 1;}} \underbrace{\mathrm{e}^{-(\omega\beta/c)\boldsymbol{r}}}_{\text{absorption; imaginary part of refraction index.}}$$

$$\beta \ll 1$$

$$\delta \simeq 1$$

$$\beta = \frac{\lambda \rho}{4\pi} (\mu / \rho)$$

mass attenuation coefficient

$$\delta = N_A \frac{Z}{A} \rho e^2 \lambda^2 / 2\pi m_e c^2$$

Avogadro's constant

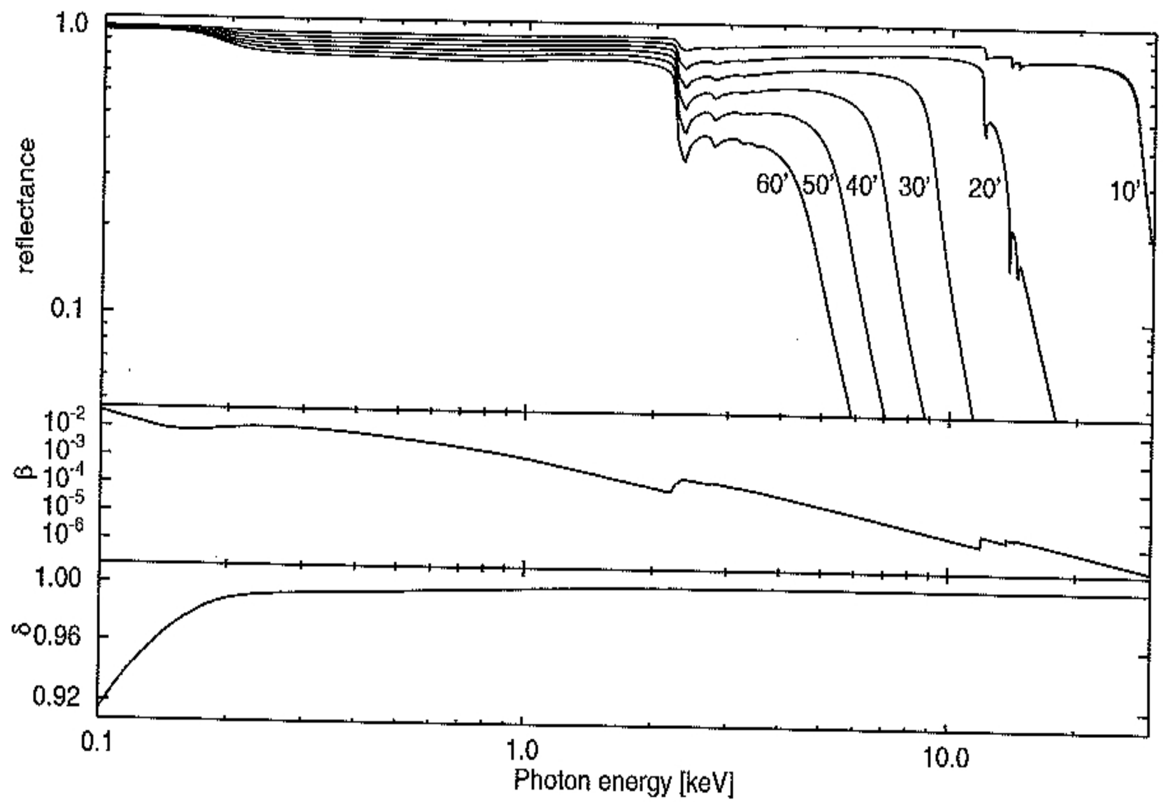

Reflectance of gold for different grazing angles, α:

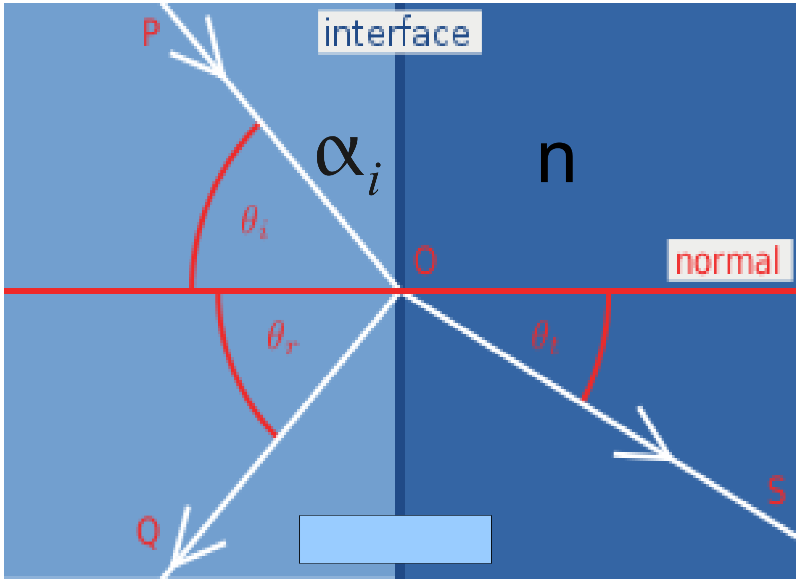

<u>Critical grazing angle:</u> α_c

<u>below which the total external reflection occurs:</u>

Snell's laws: $\sin\theta_t = \sin\theta_i / n$

$$\cos\alpha_t = \cos\alpha_i / n$$

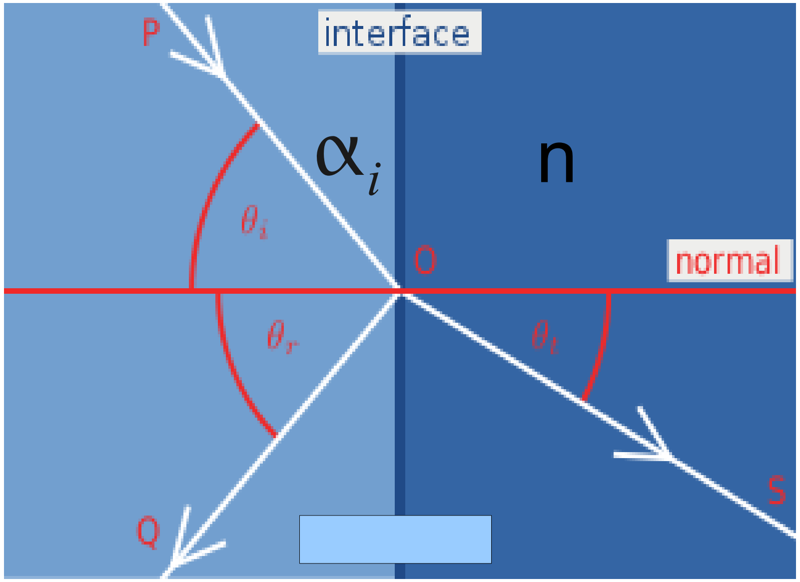

<u>Critical grazing angle:</u> α_c

<u>below which the total external reflection occurs:</u>

Snell's laws: $\sin\theta_t = \sin\theta_i / n$

$$\cos\alpha_t = \cos\alpha_i / n$$

Total external reflection when: $\alpha_i = \alpha_c$

$$\frac{\cos\alpha_c}{n} = \cos\alpha_t = 1$$

$$\cos\alpha_c = 1 - \delta$$

$$\cos\alpha_c \approx 1 - \alpha_c^2/2 = 1 - \delta$$

$$\alpha_c = \sqrt{2\delta}; \qquad \underline{\alpha_c = 69 \times \sqrt{\rho}/E}$$

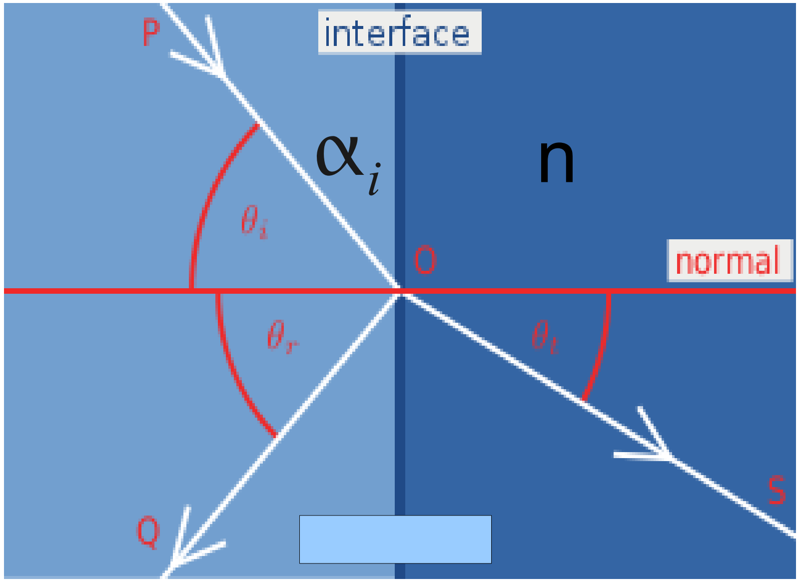

Critical grazing angle: α_c below which the total external reflection occurs:

Snell's laws: $\sin\theta_t = \sin\theta_i / n$

$\cos\alpha_t = \cos\alpha_i / n$

Total external reflection when: $\alpha_i = \alpha_c$

$$\frac{\cos\alpha_c}{n} = \cos\alpha_t = 1$$

$$\cos\alpha_c = 1 - \delta$$

$$\cos\alpha_c \approx 1 - \alpha_c^2/2 = 1 - \delta$$

$$\alpha_c = \sqrt{2\delta}; \qquad \alpha_c = 69 \times \sqrt{\rho}/E$$

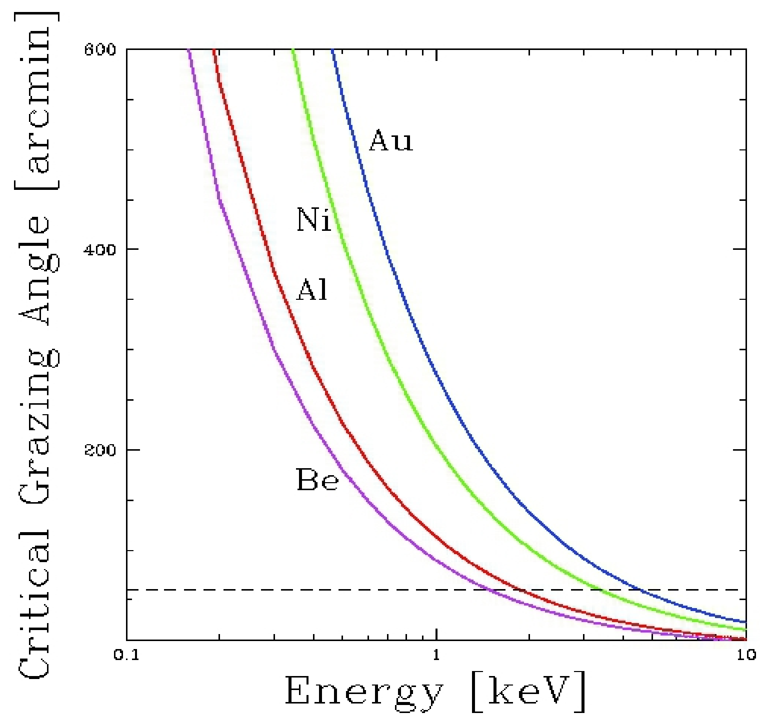

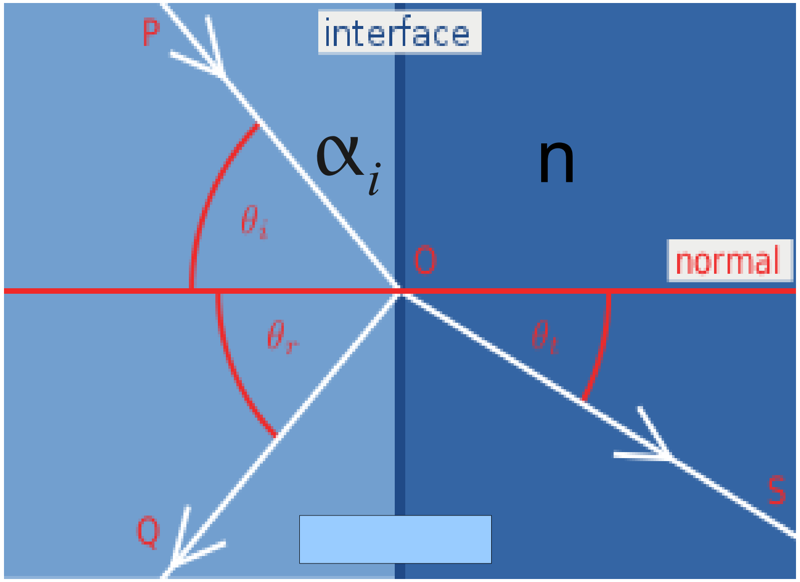

b) Fresnel's Equations:

Both: T – transmittance, and
R – reflectance, depend on
polarization of incident X-ray.

$$R_s = \left(\frac{\sin\alpha_i - (n^2 - \cos^2\alpha_i)^{1/2}}{\sin\alpha_i + (n^2 - \cos^2\alpha_i)^{1/2}} \right)^2$$

for polarization perpendicular to the plane of diagram

$$R_p = \left(\frac{(n^2 - \cos^2\alpha_i)^{1/2} - n^2\sin\alpha_i}{(n^2 - \cos^2\alpha_i)^{1/2} + n^2\sin\alpha_i} \right)^2$$

for polarization parallel to the plane of diagram

$$T_s = 1 - R_s; \qquad T_p = 1 - R_p$$

For unpolarized light: $$R = \frac{R_s + R_p}{2}$$

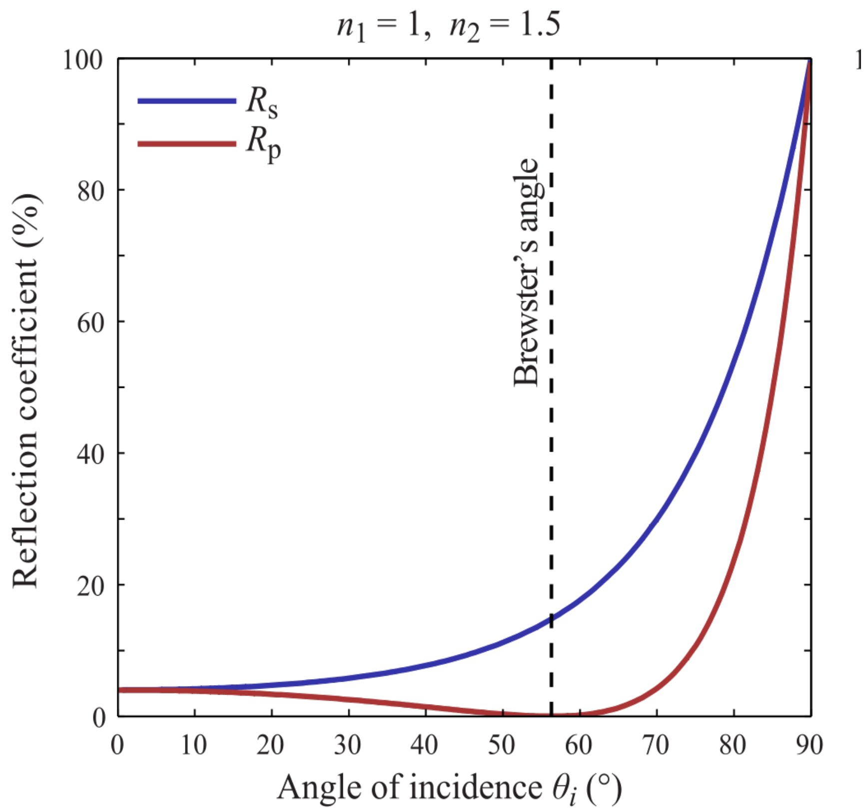

Brewster's angle for glass in air of vacuum, represents total internal reflection.

For unpolarized light:

$$R = \frac{R_s + R_p}{2}$$

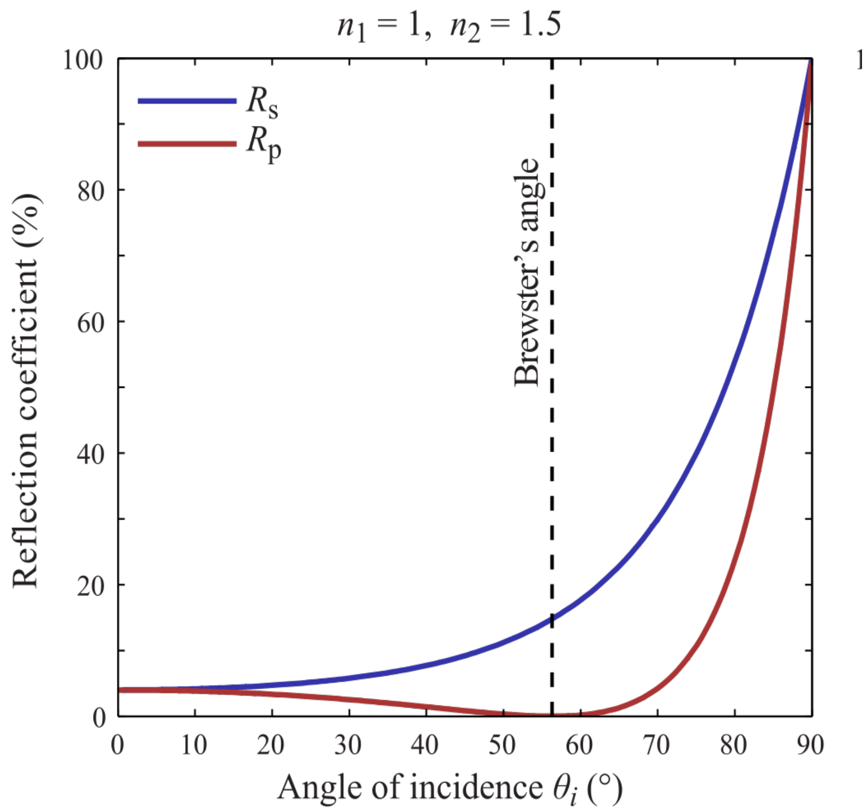

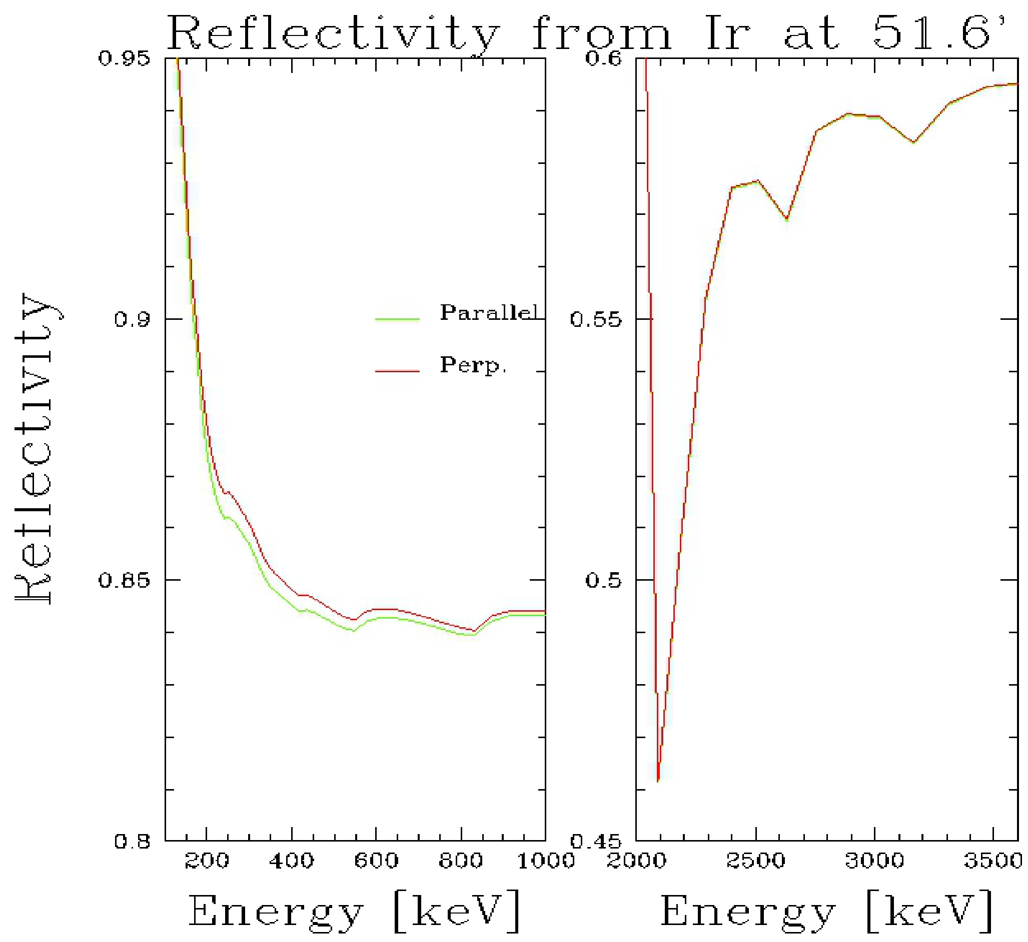

Brewster's angle for glass in air of vacuum, represents total internal reflection.

Reflectivity depends on polarization.

c) Scattering

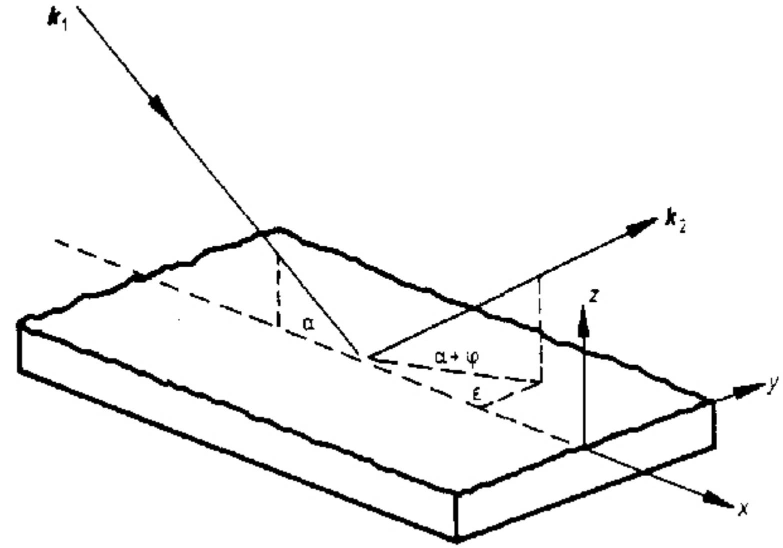

Figure 1. Scattering geometry. $\boldsymbol{k}_1$ and $\boldsymbol{k}_2$ denote the wavevector of the incident and scattered ray, respectively.

The surfaces are not infinite smooth. This gives rise to the complex subject of X-ray scattering, which cannot be treated *exactly.*

Statistical description of the surface roughness, which treads irregularities in the surface height h as random, characterized by a power spectral density function:

$$2\mathrm{W}(f) = \left| \int e^{i2\pi x f} h(x)\, dx \right|^2$$

Gives general trends:

1) Scattering increases as E^2
2) In plane scattering dominates by a factor of $1/\sin\alpha$

c) Scattering

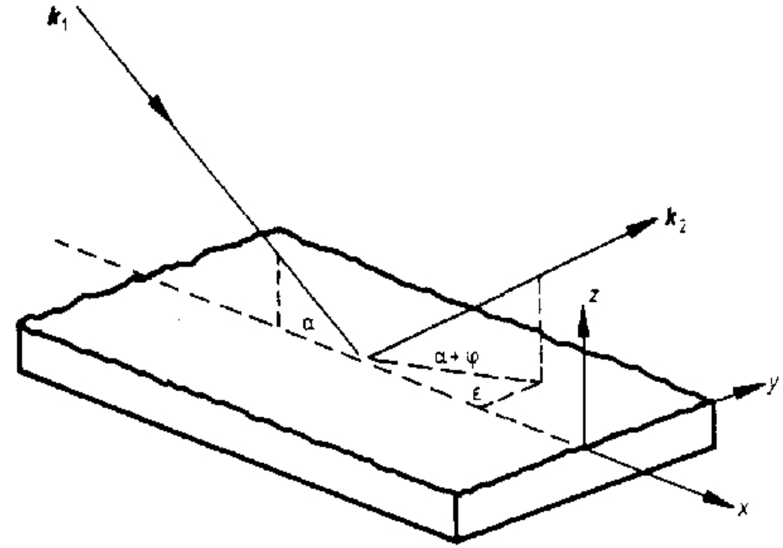

Figure 1. Scattering geometry. $\boldsymbol{k}_1$ and $\boldsymbol{k}_2$ denote the wavevector of the incident and scattered ray, respectively.

The surfaces are not infinite smooth. This gives rise to the complex subject of X-ray scattering, which cannot be treated *exactly.*

Statistical description of the surface roughness, which treads irregularities in the surface height h as random, characterized by a power spectral density function:

$$2W(f) = \left| \int e^{i2\pi x f} h(x)\, dx \right|^2$$

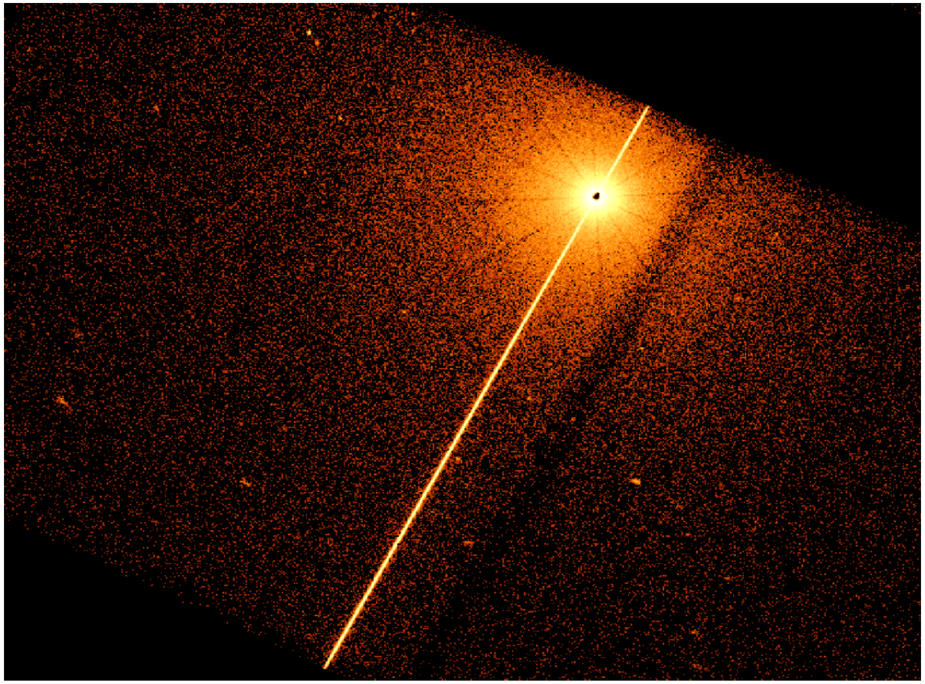

Gives general trends:

1) Scattering increases as E^2
2) In plane scattering dominates by a factor of $1/\sin\alpha$

Interface from a vacuum to an reflected layer is not perfect:

The mirror substrate material; e.g., Zerodur for CHANDRA,
A thin binding layer e.g., Chromium, to hold the heavy metallic coating to the glass,
The high Z metal coating; e.g., Iridium for CHANDRA
Overcoat of molecular contaminants *****

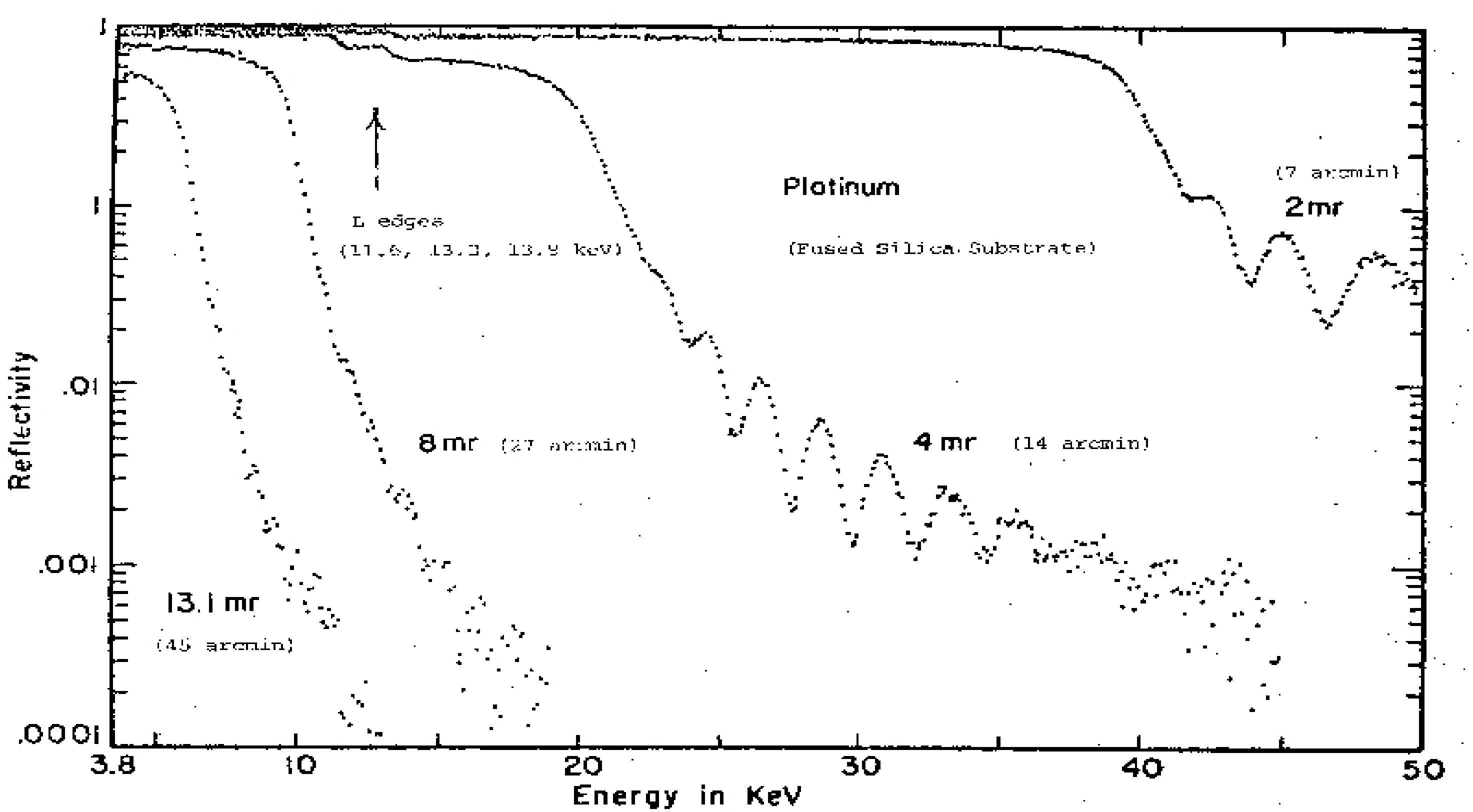

Figure 3.2 The reflectivity of a platinum coated mirror as a function of energy and grazing angle.

d) Mirror's figure

For optical mirrors of spherical shape, Abbe's condition is satisfied:

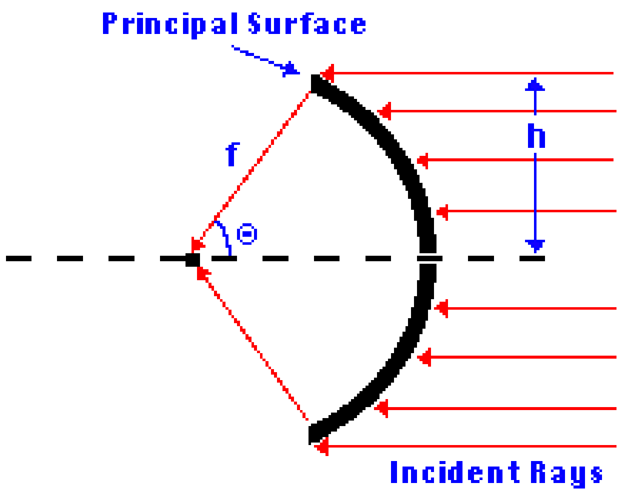

$$\frac{h}{\sin\theta} = f$$

For mirror with parabolic shape Abbe's condition does not work.

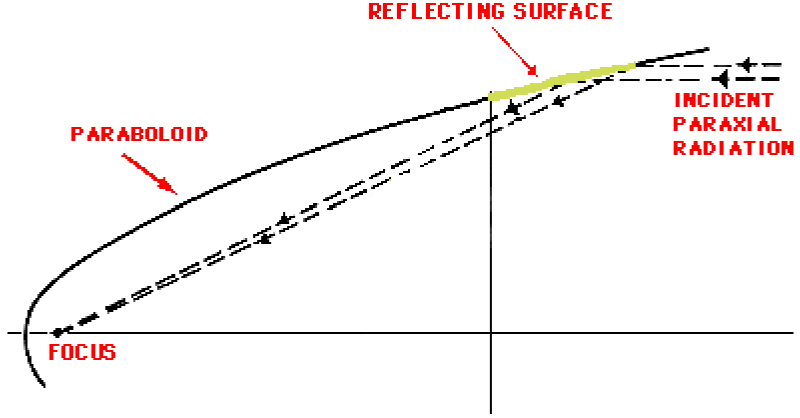

Grazing incident X-ray mirrors – Wolter pointed out that *two* mirrors of the different figures of revolution, fulfills the sine condition *exactly for on-axis rays.*

1952 , Annalen der Physik

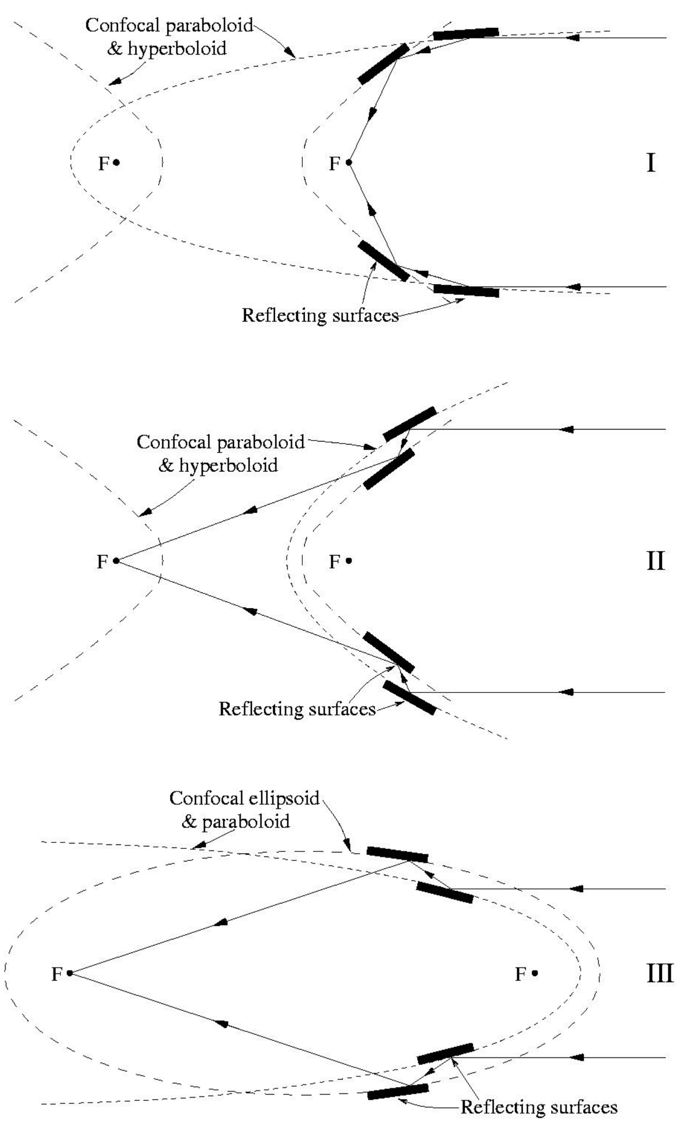

Type I – paraboloid + hyperboloid
allows for nested mirrors,
most commonly used

Type II – paraboloid + hyperboloid
no nesting, more compact
for Solar X-ray Telescope

Type III – paraboloid + ellipsoid
never used.

Solution for X-ray Wolter's optic:

at least two mirrors,
even number of mirrors can satisfy the sine condition,
odd numbers of mirrors *cannot,*
two mirror systems are strongly favored, because four, or more would increase the losses due to scattering and reflection,
alignment of more than two mirrors is complicated,
nested mirrors.

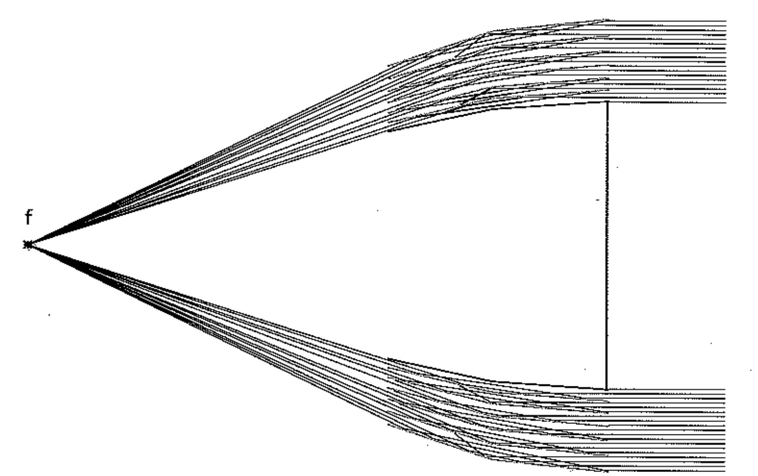

Fig. 6.7 Nested Wolter-1 mirror shells provide large effective apertures; as nested shells act as aperture stops, they limit the field-of-view but can also prevent direct light and singly reflected rays from penetrating the mirror system

Wolter Type I Mirror System:

α - small $\rightarrow$ f - large focal axis

$$r / f = \sin 4\alpha$$

2r/f typically about 1/10
for E up to 10 keV,
assuming $\alpha < 1°$

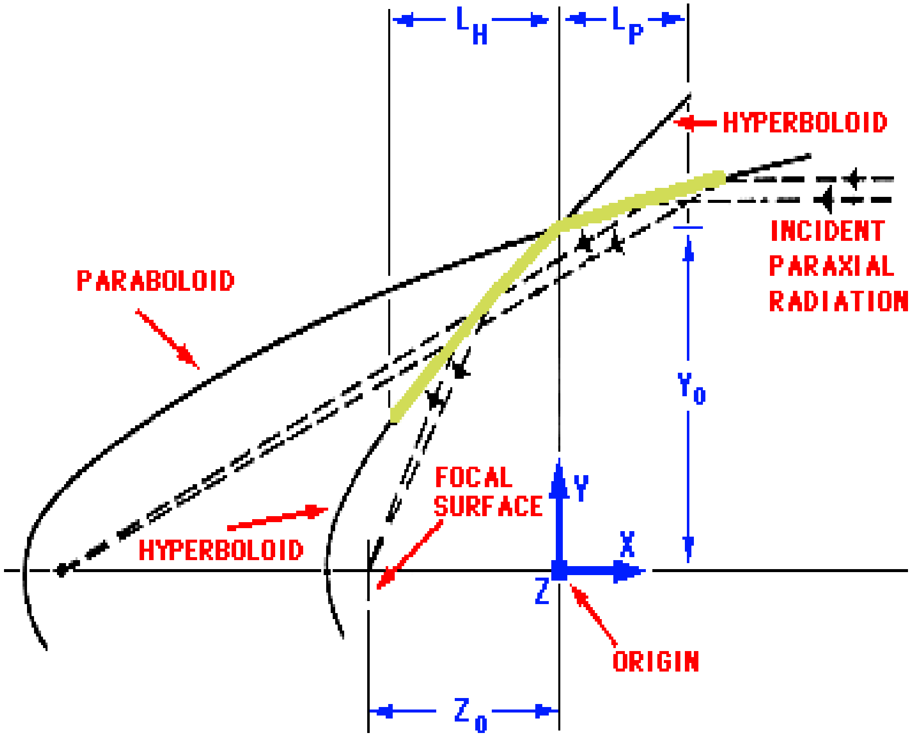

2r – mirror diameter limited by both: by geometrical vignetting, and the shape of the reflecting surface, lower ratio of 2r/f results in smaller FOV.

ROSAT PSPC – FOV 2°
XMM-Newton – FOV 30'

Wolter Type I Mirror System: Off-Axis angle

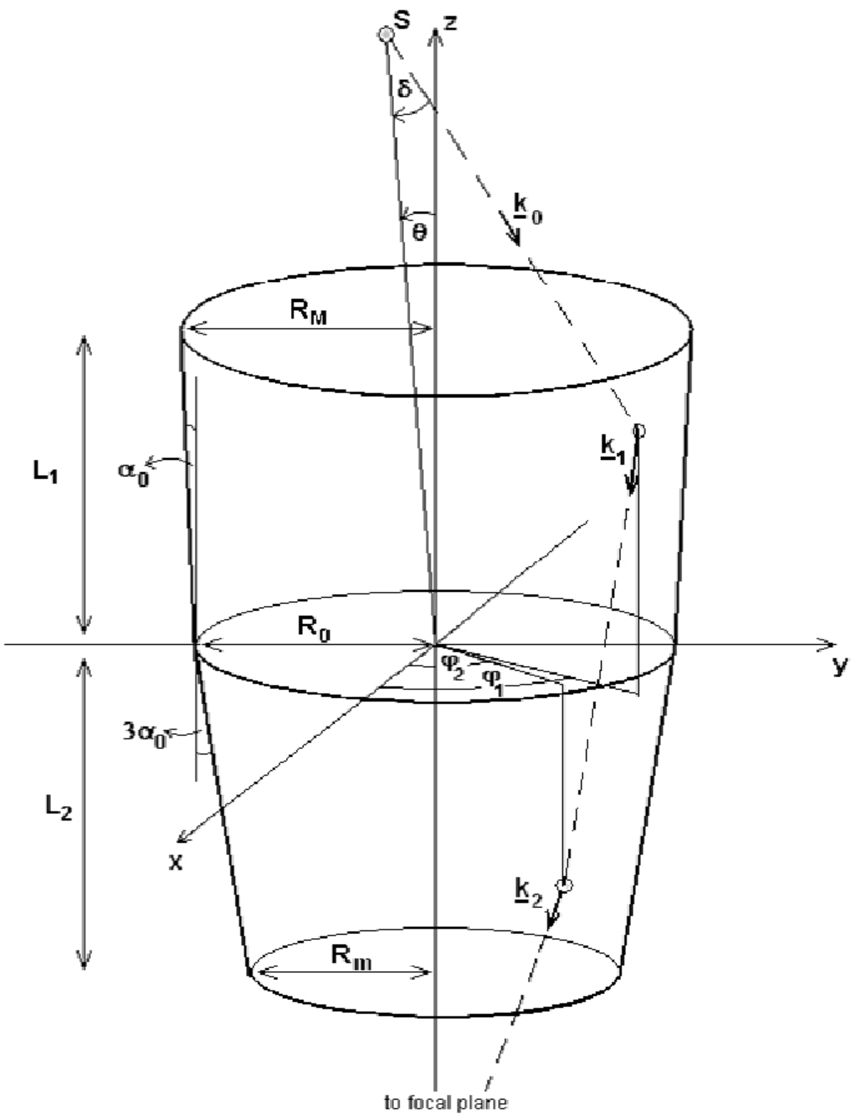

Fig. 1. Sketch of a grazing-incidence Wolter-I mirror shell with an off-axis X-ray source. We also show a ray direction vector before reflection ($\underline{k}_0$), after the first reflection ($\underline{k}_1$), and after two reflections ($\underline{k}_2$).

θ - angle between incident X-rays and optical axis,

Image quality degrades continuously with increasing off-axis angle.

Wolter Type I Mirror System: RMS Blur Circle radius

α_p - paraboloid slope angle,

α_h - hyperboloid slope angle,

$$\xi = \alpha_p / \alpha_h$$ (1 for most missions)

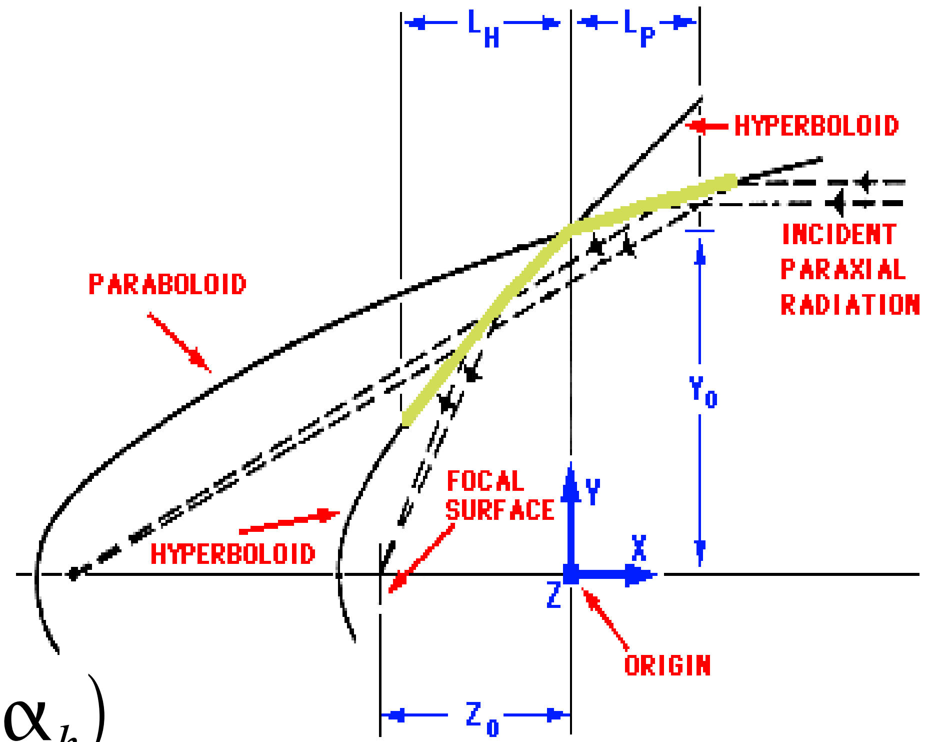

$$\alpha = \frac{1}{4}\tan^{-1}(Y_0 / Z_0) = \frac{1}{2}(\alpha_p + \alpha_h)$$

Empirical formula for the RMS Blur Circle radius:

$$\sigma = \frac{(\xi + 1)}{10} \times \frac{L_p}{Z_0} \times \frac{2\tan^2\theta}{\tan\alpha} + 4\tan\theta\tan^2\alpha$$

Wolter Type I Mirror System: RMS Blur Circle radius

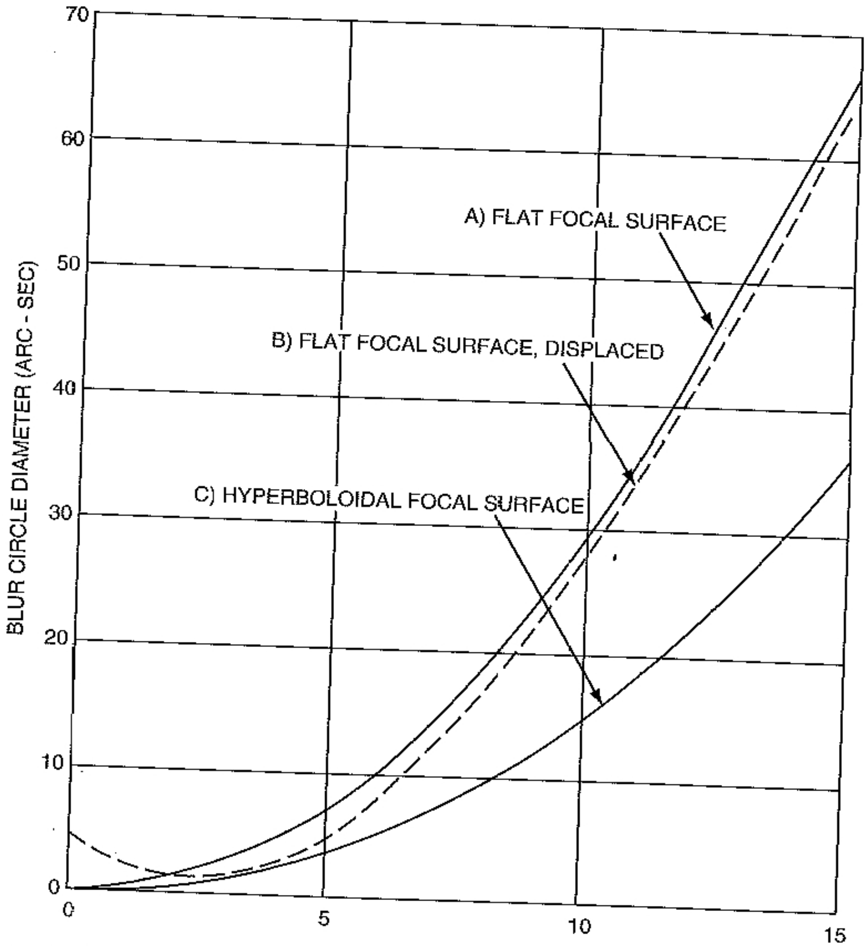

Fig. 6.6 Total blur circle diameter vs. off-axis angle in arcminutes, from a ray tracing done on a telescope system with $2r/f = 1/10$ and $l = 2r$; the detector shift is $0.00018f$ (from Giacconi et al. [7])

Giacconi et al. 1969

Optimal focal surface is a bowl shape, sitting on a flat plane perpendicular to the optical axis

Wolter Type I Mirror System: RMS Blur Circle radius

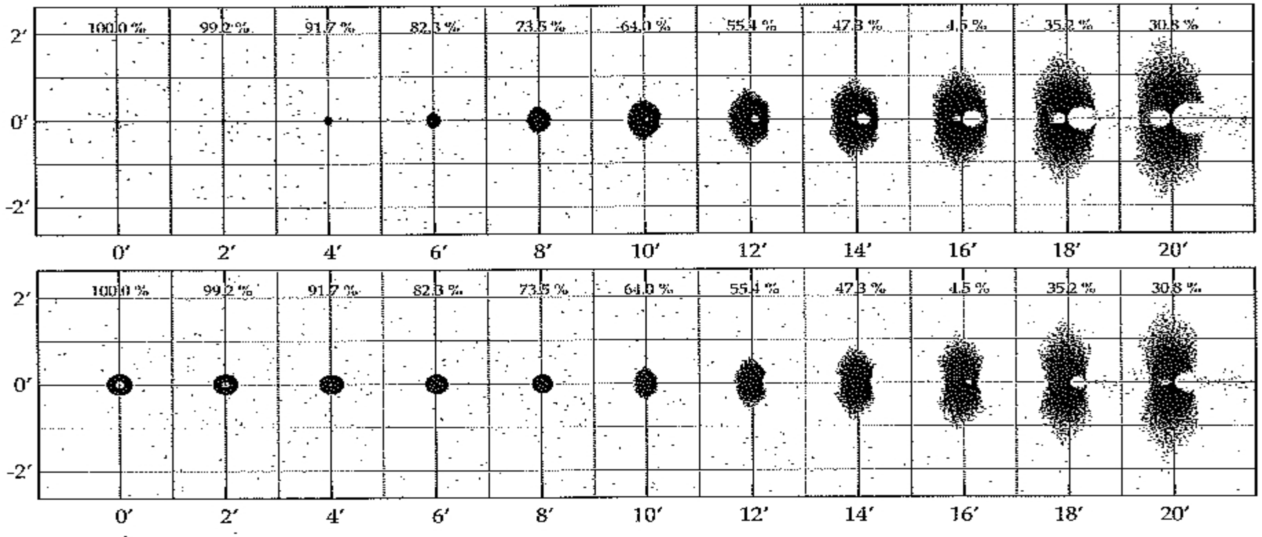

unshifted detector plane

shifted detector plane

Fig. 6.5 Ray tracing calculated point spread function for off-axis angles from 0′ to 20′ for a nested mirror system with $2r_{\max}/f = 1/10$ and $l = 1.8r_{\max}$ with an unshifted detector plane (*upper panel*) and with a shifted one – the shift is $0.00125f$ (*lower panel*); the percentage numbers denote the vignetting

Collecting area:

For the small grazing angle the geometrical area of the mirror shell is a thin circle with an projected area *A*:

$$A \simeq 2\pi Y_0 \times L_p \tan\alpha$$

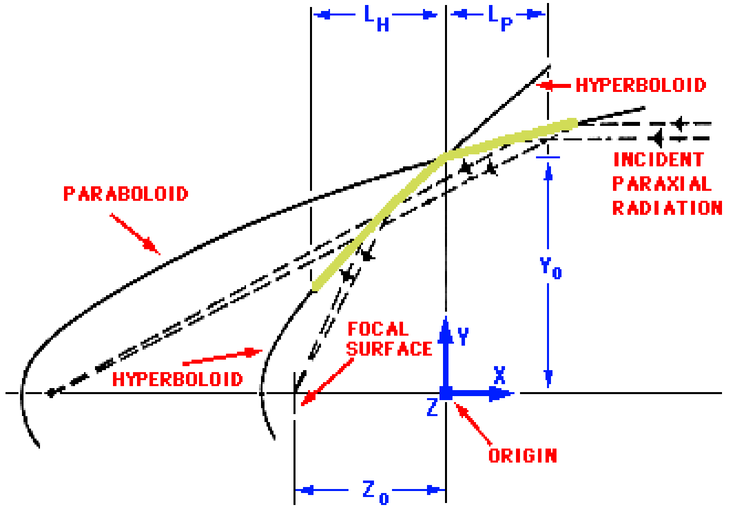

Effective collecting area A_{eff}:

$$A_{eff}(\alpha, E) \simeq A R^2(\alpha, E) \simeq 8\pi Z_0 L_p R^2(\alpha, E)\alpha^2$$

Fresnel reflectivity

Nesting – solution for enlarged effective collecting area.

58 nested mirrors in XMM-Newton:

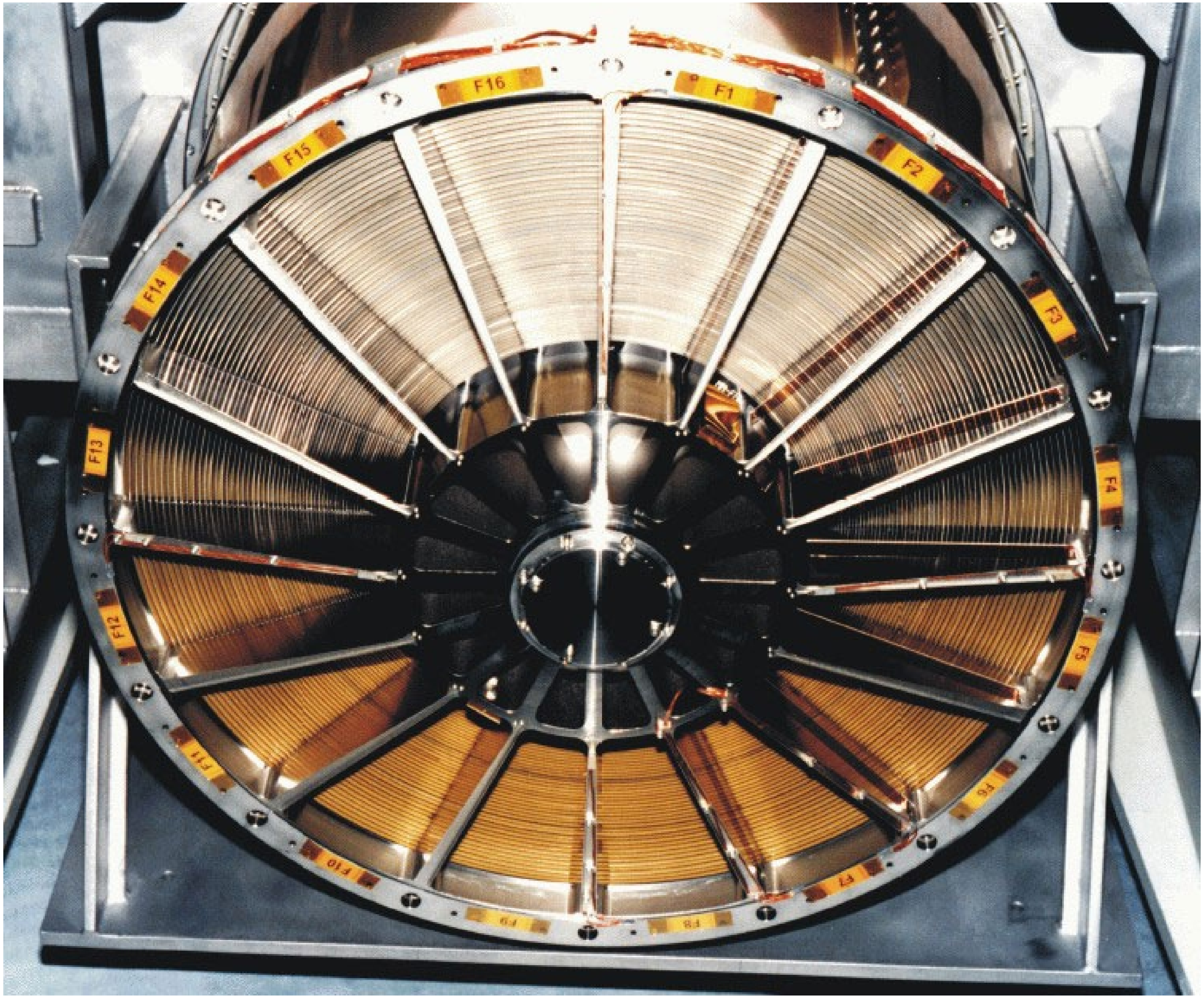

XMM–Newton

X–Ray Multi Mirror – Röntgen Satelliten Observatorium der ESA

(Posterdesign: IAAT / 2006 – schanz@astro.uni-tuebingen.de, tenzer@astro.uni-tuebingen.de)

XMM Start

Der Start von XMM war am 10. Dezember 1999 mit einer Ariane 5 G Trägerrakete von Kourou, Französisch–Guayana aus.

XMM im Überblick:

Start:	10. Dezember 1999
Nutzlast:	3 EPIC (European Photon Imaging Camera) Kameras, davon zwei MOS–CCD Kameras eine pn–CCD Kamera 2 Reflection Grating Spectrometer (RGS) optischer Monitor (OM)
Abmessungen:	4m x 4m x 10m, Spannweite der Solarflügel: 16 m
Startmasse:	3,8 Tonnen
Orbit:	Perigäum: 7000 km, Apogäum: 114000 km, Inklination: 40°, Periode: 48 Stunden
Optik:	3 tonnenförmige Spiegelmodule, bestehend aus je 58 Wolter–Spiegeln, Brennweite: 7,5 m
Auflösung:	6 Bogensekunden
Spektralbereich:	0,1 bis ca. 15 keV
Missionsdauer:	bis zu 10 Jahre

XMM Orbit

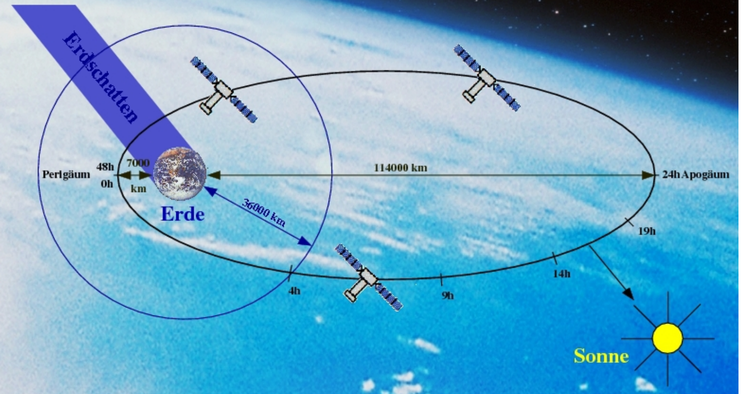

Die Umlaufbahn von XMM ist stark exzentrisch und hat eine Umlaufzeit von ca. 48 Stunden. Der erdnächste Punkt (Perigäum) liegt bei einem Abstand von 7000 km, der erdfernste Punkt (Apogäum) bei etwa 114000 km. Die Umlaufbahn ermöglicht lange ununterbrochene Beobachtungen außerhalb des Strahlungsgürtels der Erde.

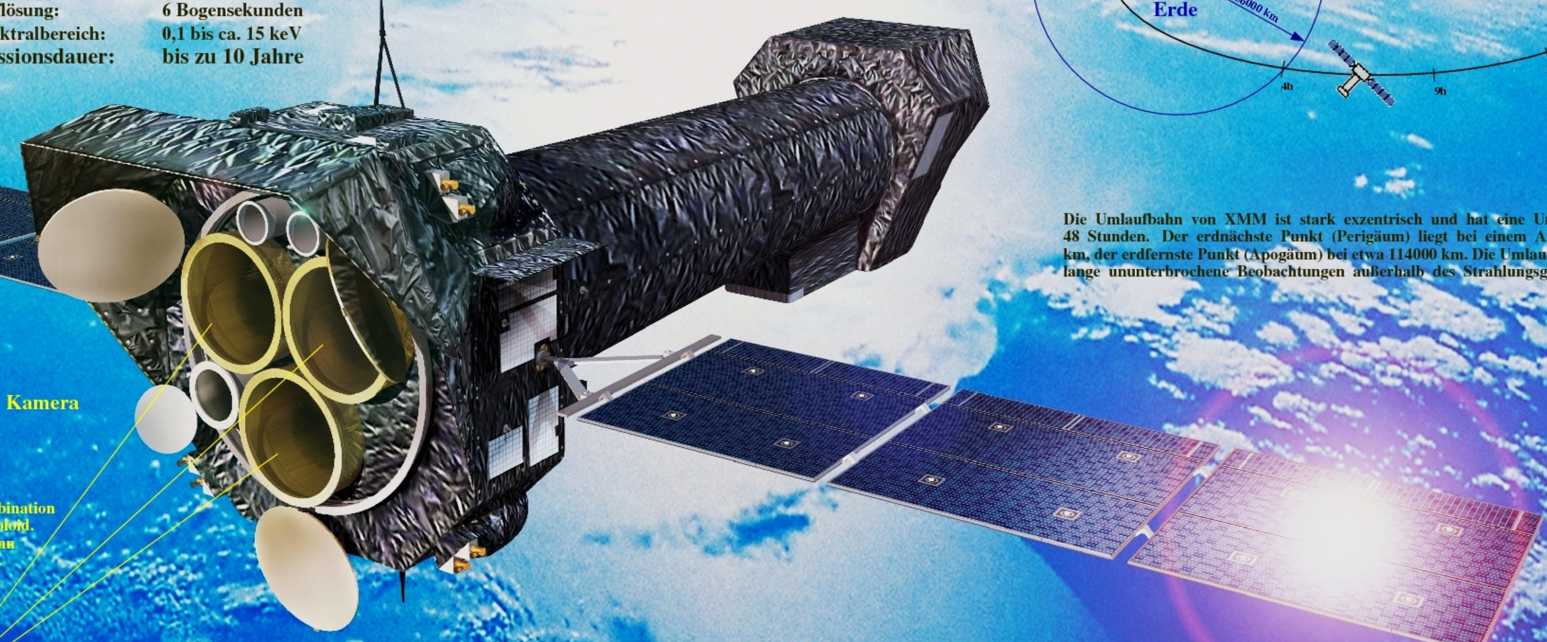

Wolter–Teleskope

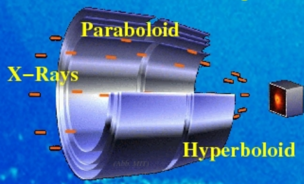

Ein Wolter–Teleskop besteht aus einer Kombination von einem Paraboloid und einem Hyperboloid. Das Röntgenlicht wird nur reflektiert, wenn es in einem flachen Winkel streifend einfällt. Durch eine schichtweise Anordnung der Spiegel kann die Spiegeloberfläche stark vergrößert und die Lichtausbeute um ein Vielfaches erhöht werden.

Wolter–Spiegel

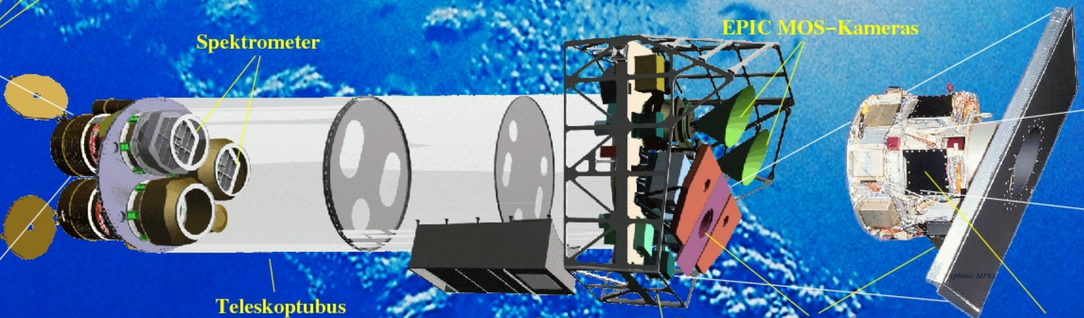

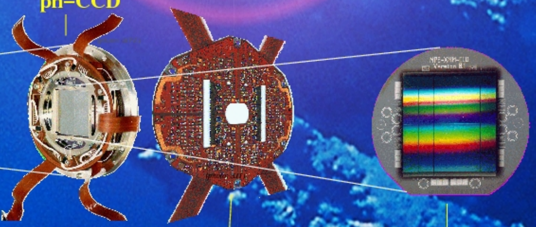

Jedes der drei Wolter–Teleskope von XMM besteht aus 58 Gold bedampften Nickelspiegeln, die wie Zwiebelschalen angeordnet sind und insgesamt eine Spiegelfläche von 120 Quadratmetern ergeben.

Durch den Teleskoptubus gelangt das Röntgenlicht in den Instrumententräger. Dort befinden sich zwei MOS–CCD Kameras und eine Silizium pn–CCD Kamera, die am MPE Garching entwickelt wurde. Die Kameras befinden sich im Fokuspunkt der Wolter–Spiegel bei einem Abstand von 7,5 Metern.

Der Kamerakopf der pn–CCD Kamera enthält die Kamera–Elektronik und das pn–CCD. Unser Institut (IAAT) war an der Entwicklung der Elektronik und der Auswertesoftware der pn–CCD Kamera beteiligt.

Das pn–CCD ist für die Aufzeichnung von Röntgenlicht optimiert. Es befindet sich im Kamerakopf auf einer speziell entwickelten Trägerplatine, von der es mit Steuersignalen versorgt wird. Das pn–CCD besteht aus vier Quadranten die aus jeweils 192 x 200 Pixeln bestehen, insgesamt 384 x 400 Pixeln.

X-ray focal image of the mirror shell 57 (D=30cm) measured at Al Kα (1.49 keV), radius = 8.2 arcsec.

PANTER X-ray Test-Facility, MPE.

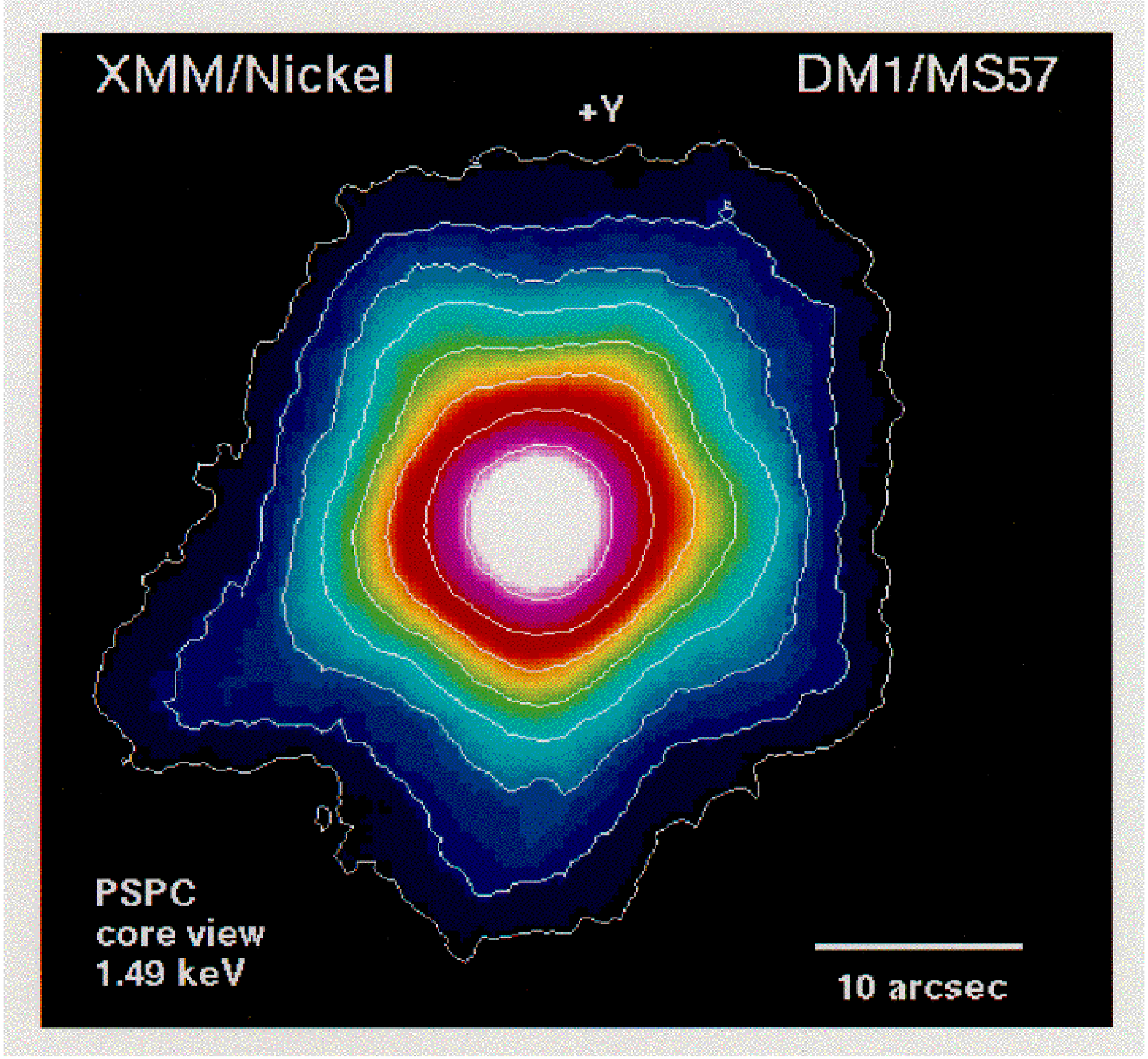

120 meter
distant
point source,

Infocal and extrafocal images show structure due to the mirror shells and residual structure of the image at the focal position.

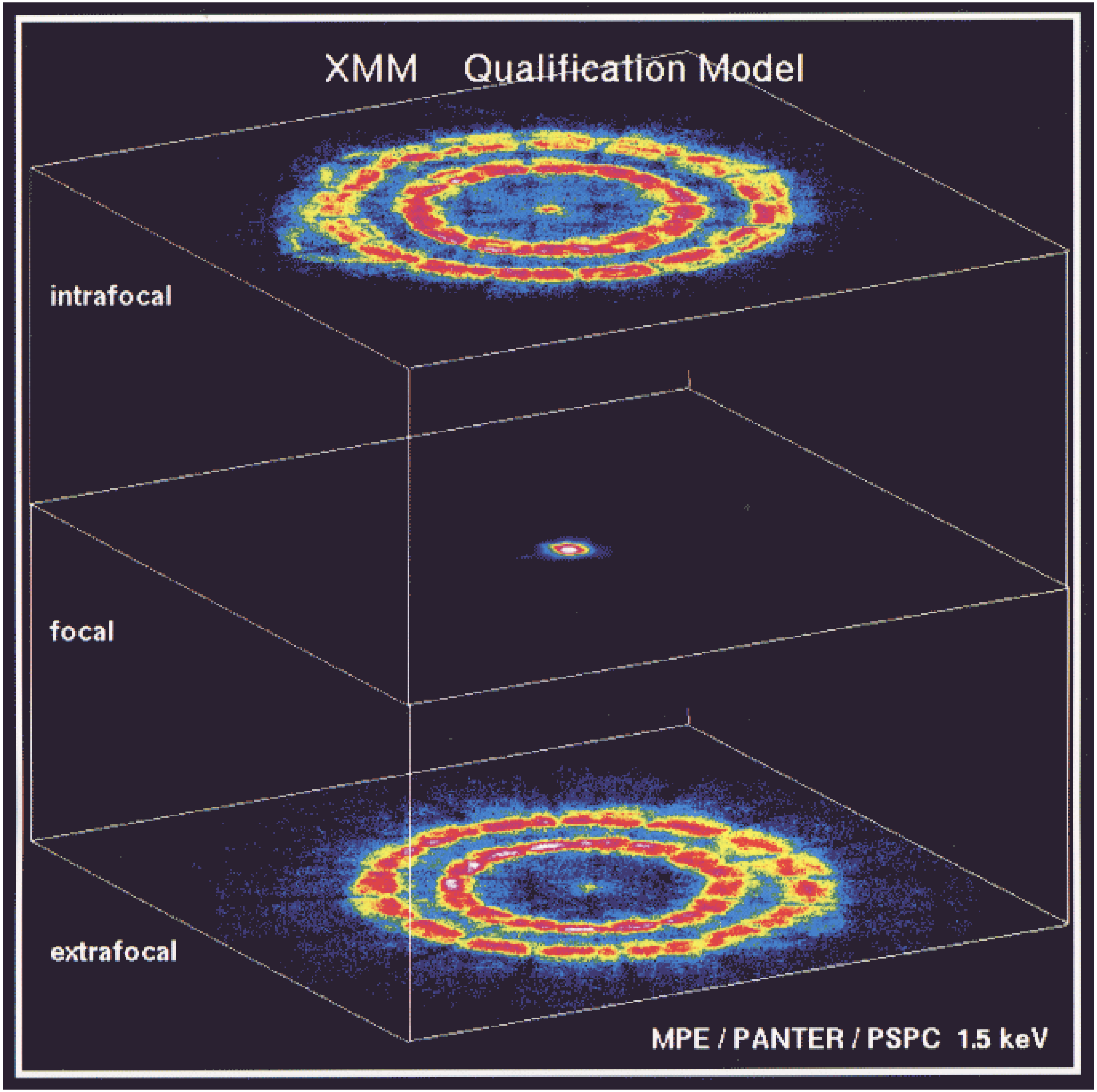

PANTER first light log-scaled intensity image for the point source at 8 keV. 10 x 6 arcmin, radius – 7-8 arcsec.

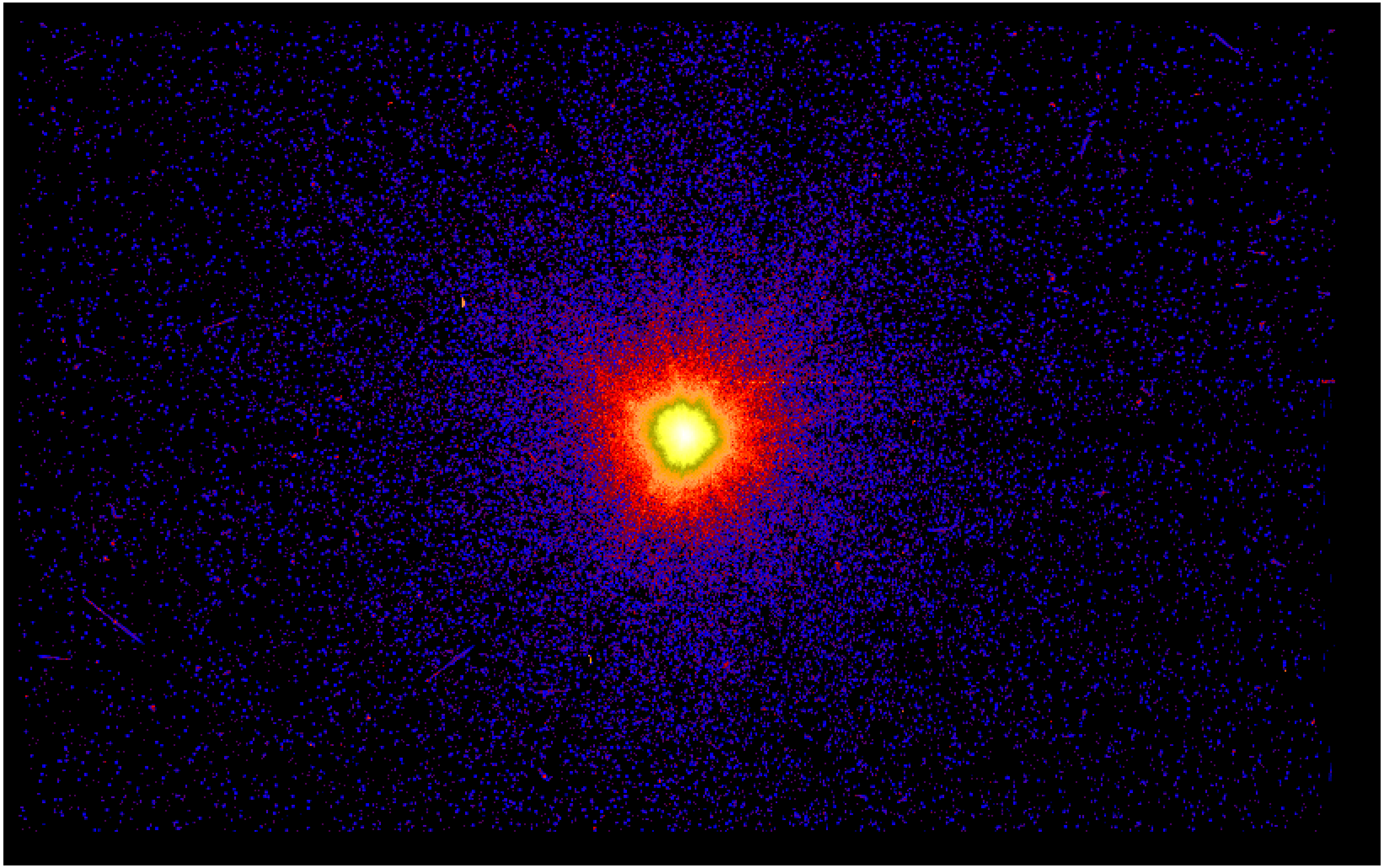

eROSITA – German Russian satellite

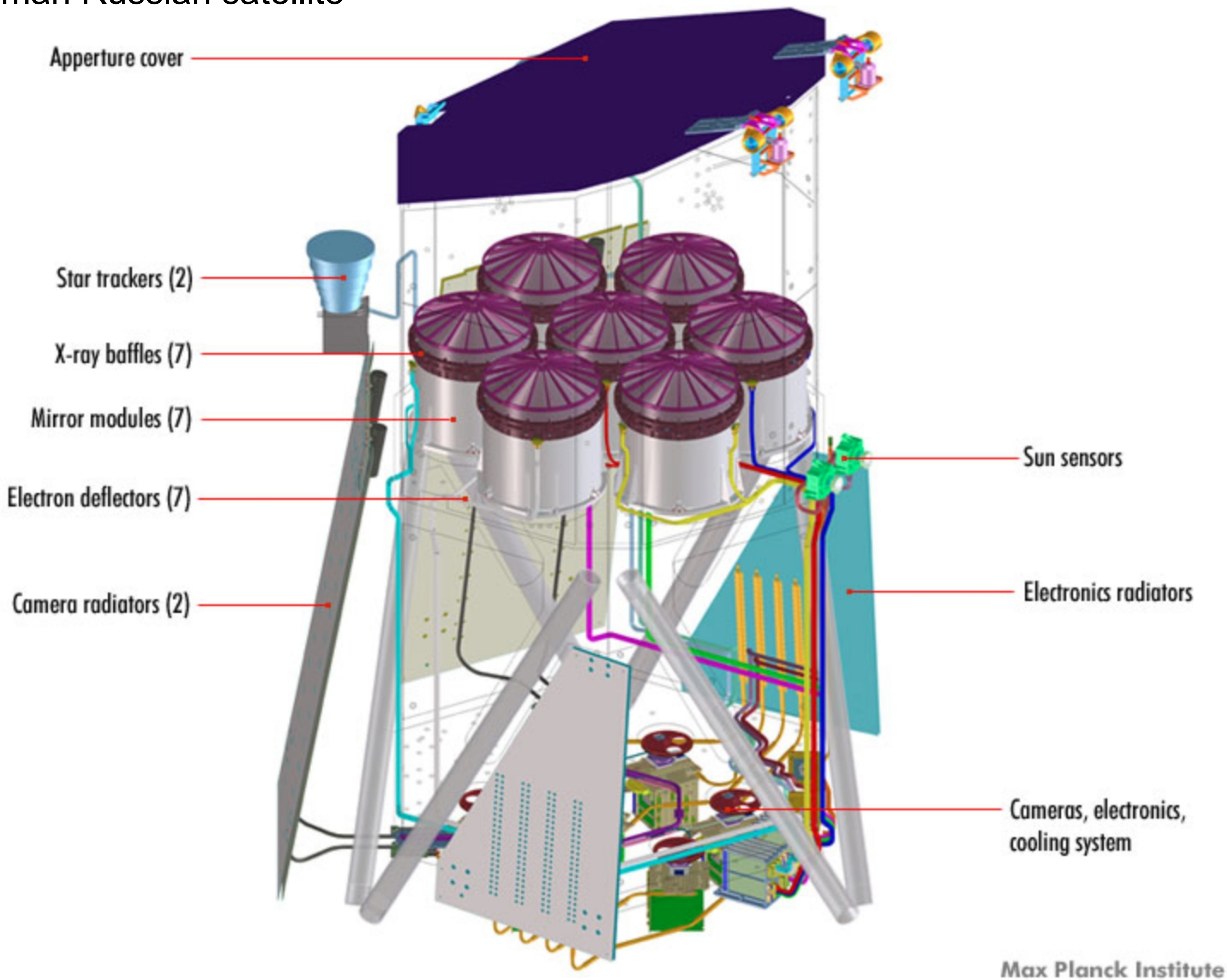

eROSITA at a glance (as of 2019):

Mirror structure	Wolter-1

Predehl et al. 2021

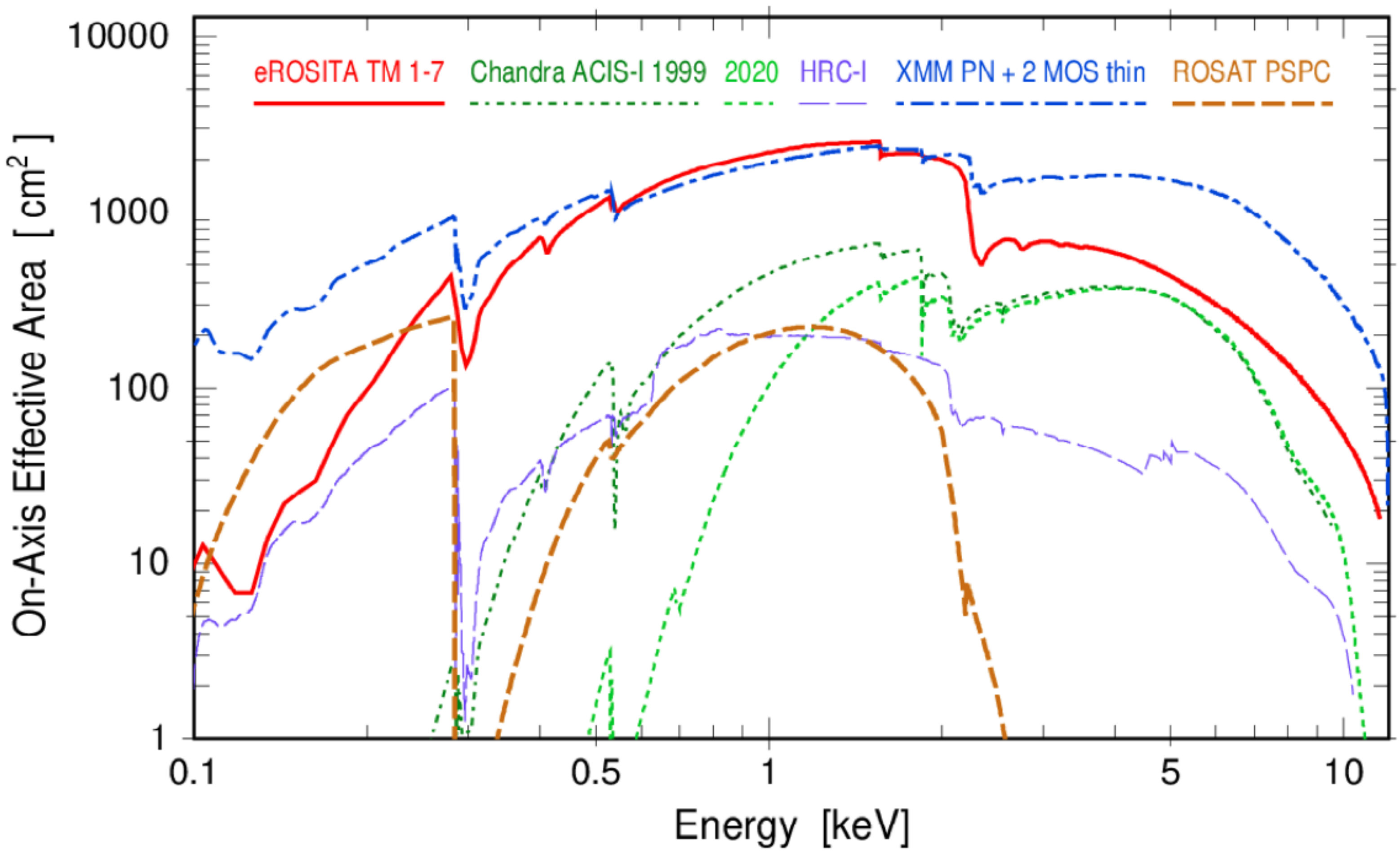

Fig. 9. Comparison of the on-axis effective areas as a function of energy for eROSITA (red), *Chandra* ACIS-I (in 1999, dark green, and in 2020, light green), *Chandra* HRC-I (purple), *XMM-Newton* (blue), and ROSAT (brown).

ATHENA Mirror Assembly –new technology Silicon Pore Optic - SPO

Dick Willingale 2019

Mirror V2.4 – 15 rows, 6 sectors

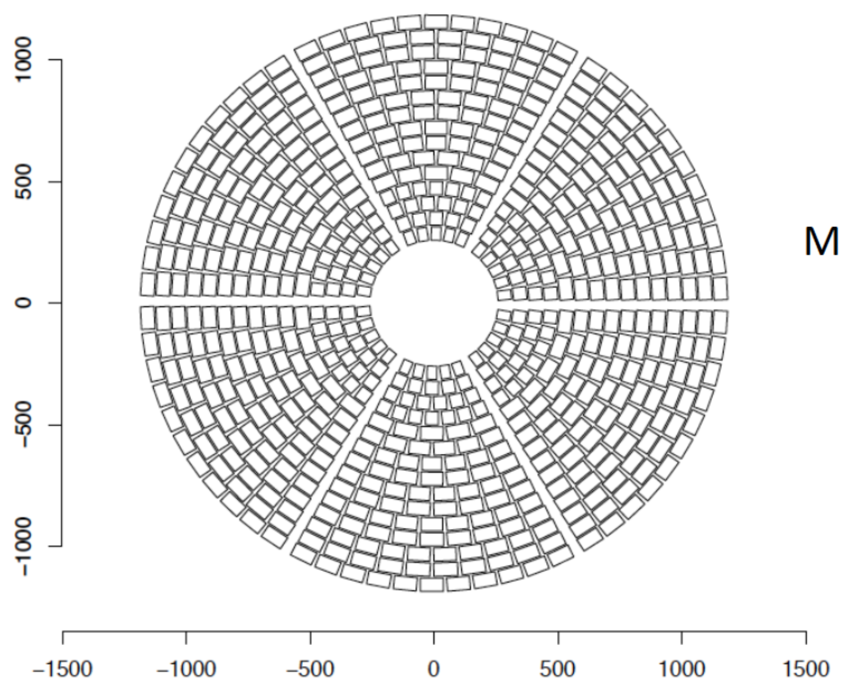

678 SPO modules

Maximum azimuthal width of module plates
100 mm r>500 mm
60 mm r<500 mm

Spherical principal plane
SPO axial length ~1/r

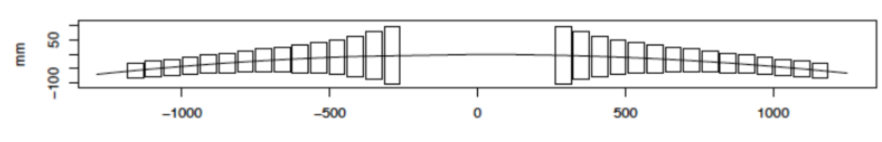

ATHENA Mirror Assembly – one module

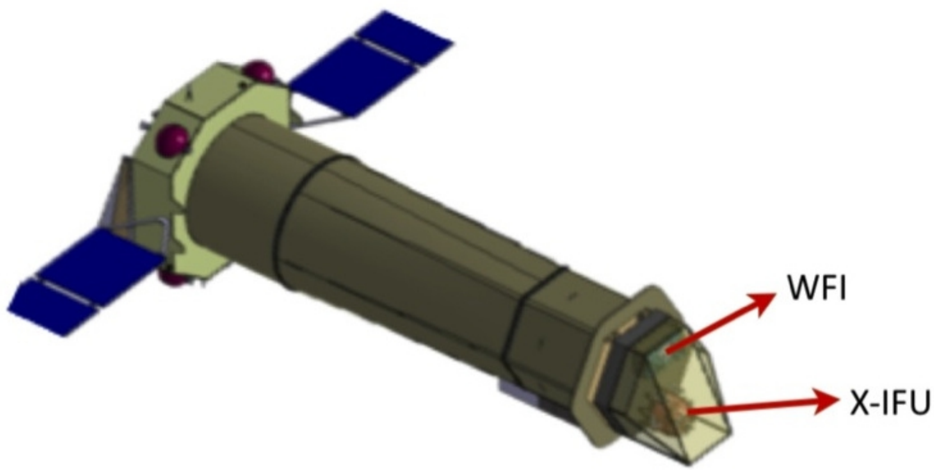

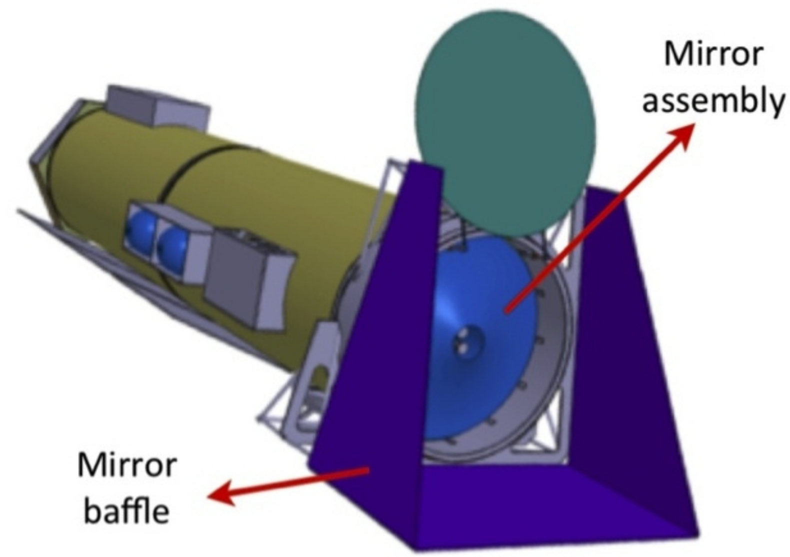

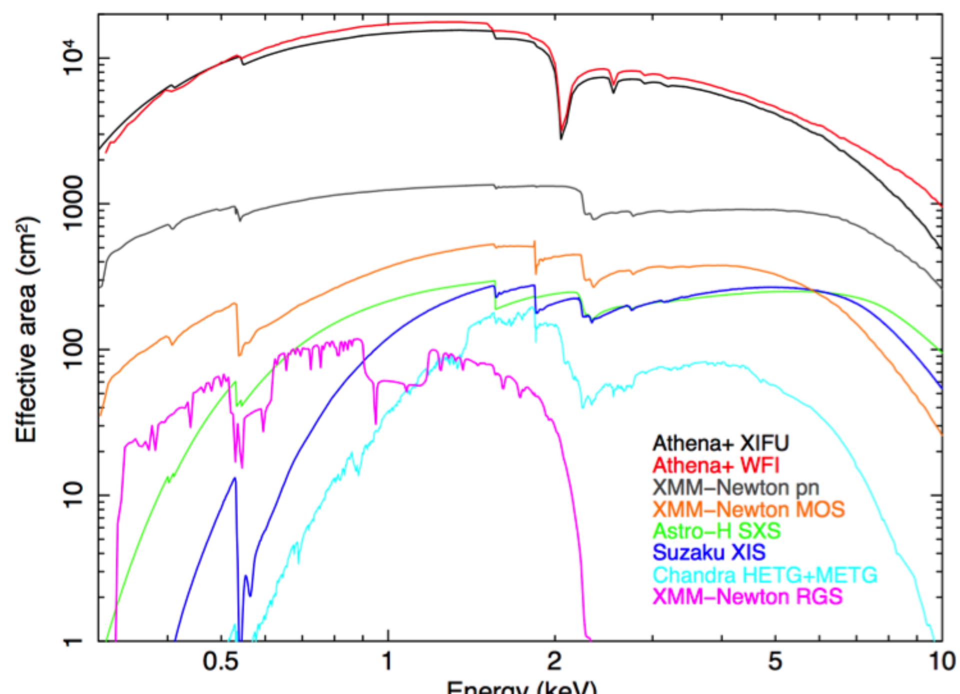

ATHENA – 2014

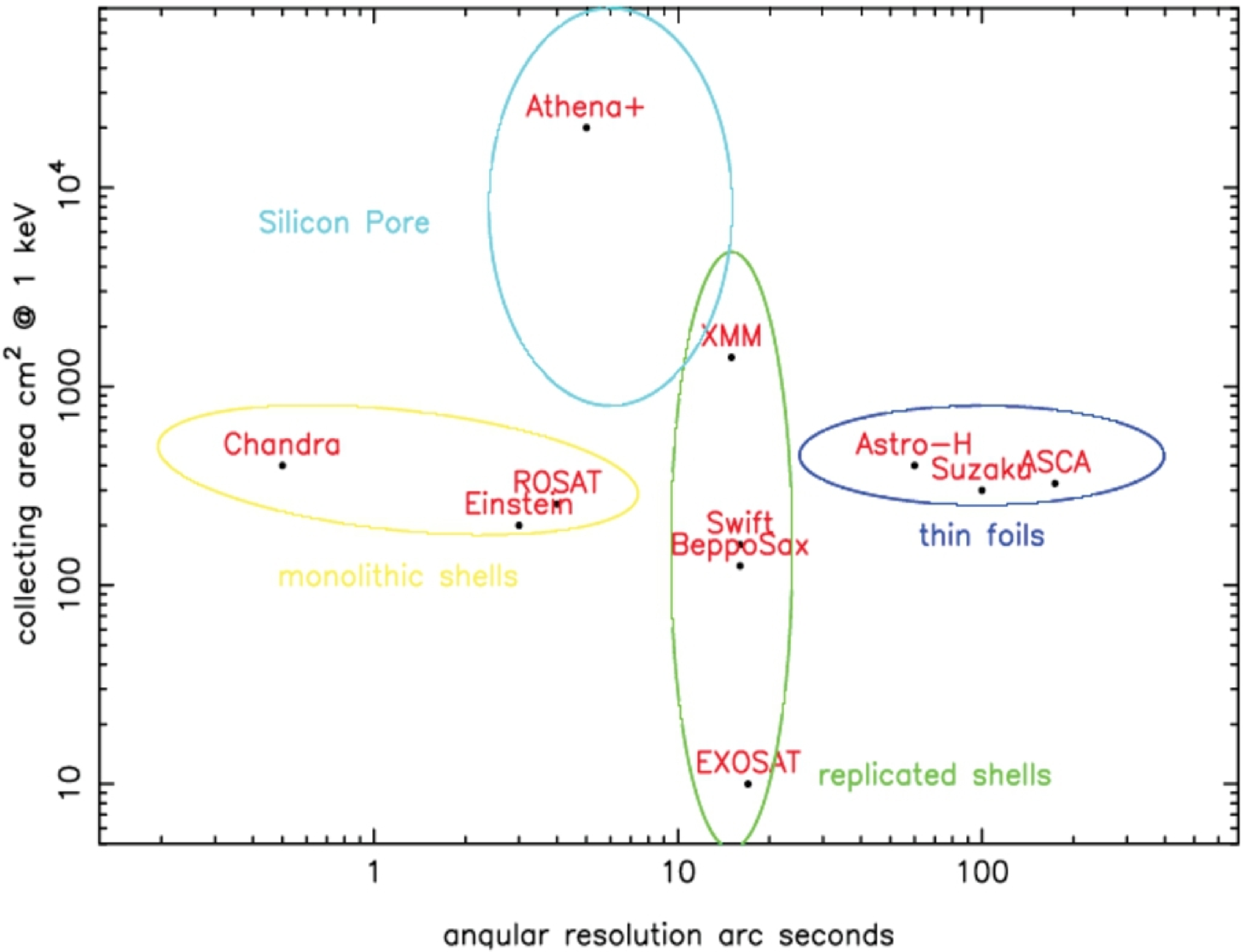

Athena+
Silicon Pore
XMM
Chandra
ROSAT
Einstein
monolithic shells
Astro-H
Suzaku
ASCA
thin foils
Swift
BeppoSax
EXOSAT
replicated shells
collecting area cm^2 @ 1 keV
10^4
1000
100
10
1
10
100
angular resolution arc seconds

ATHENA – 2014

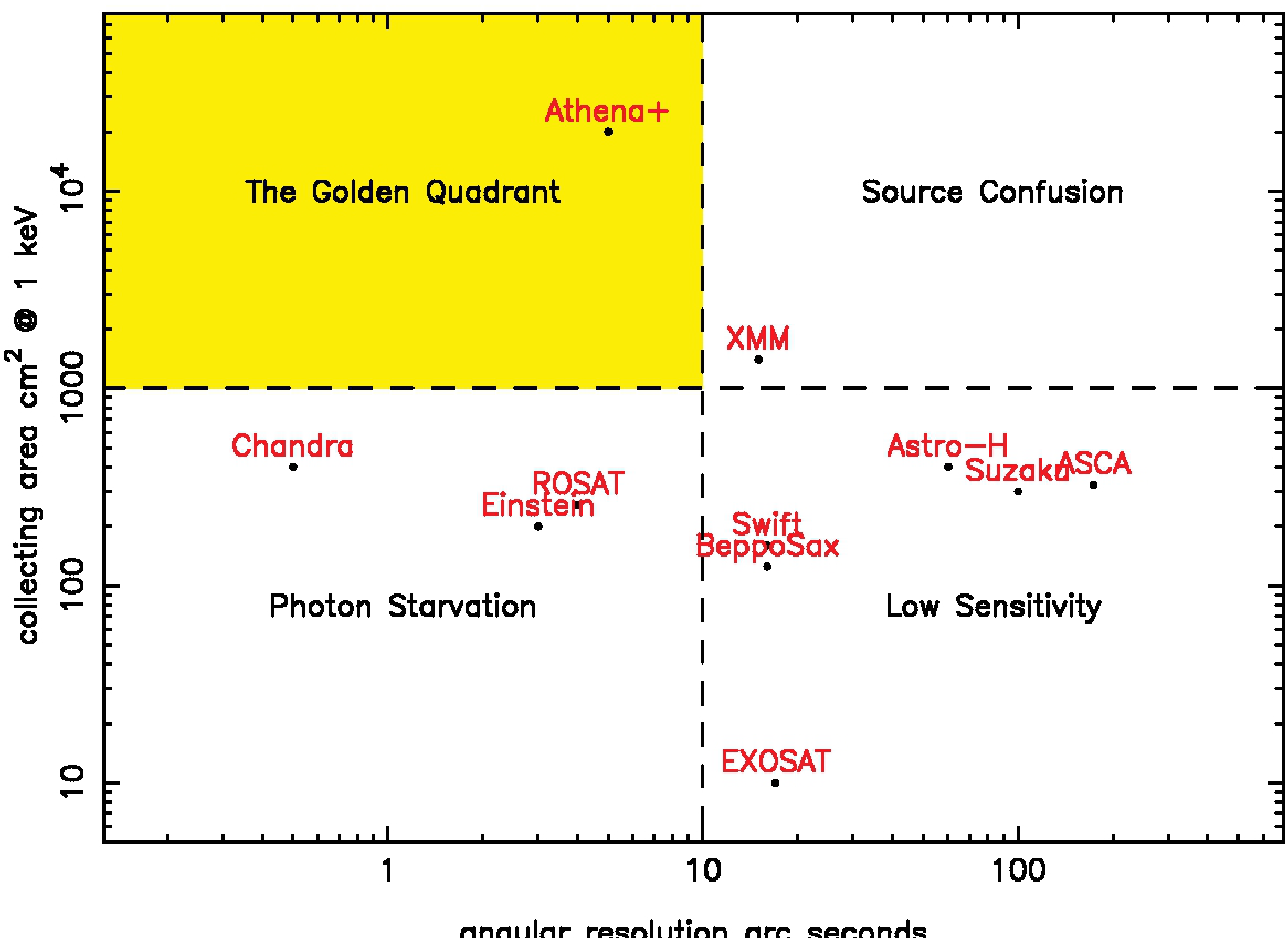

Athena+
The Golden Quadrant
Source Confusion
XMM
Chandra
Astro−H
Suzaku
ASCA
ROSAT
Einstein
Swift
BeppoSax
Photon Starvation
Low Sensitivity
EXOSAT
collecting area cm^2 @ 1 keV
10^4
1000
100
10
1
10
100
angular resolution arc seconds

ATHENA Mirror Assembly – new technology Silicon Pore Optic - SPO

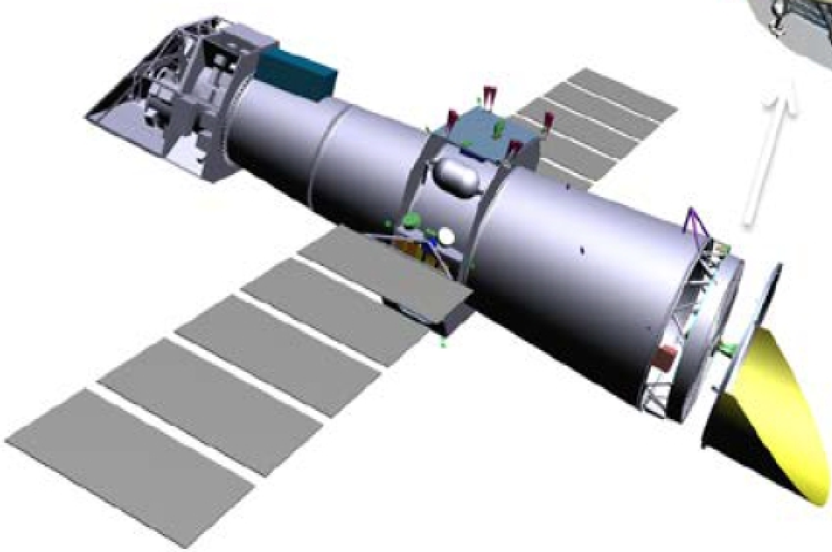

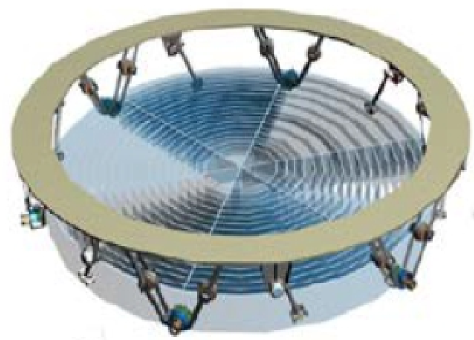

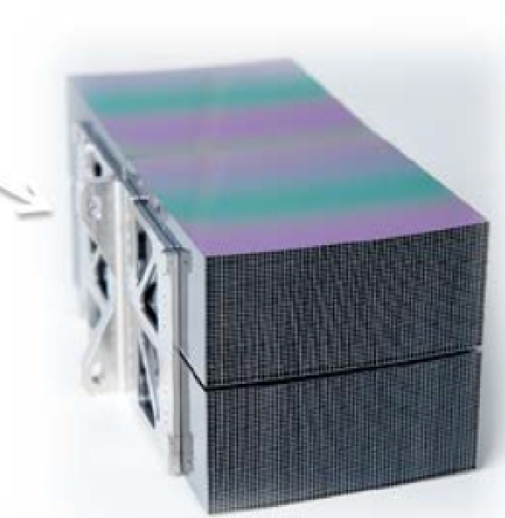

Athena mirror:

678 mirror modules
~ 100,000 mirror plates
~ 300 m^2 polished and coated area

⇒ 2 MM / day
⇒ (assuming 8h/d, 180 d/y, all MMs in 2 years)

ATHENA Mirror Assembly – problems

Stray X-ray flux from a point source outside the WFI FOV

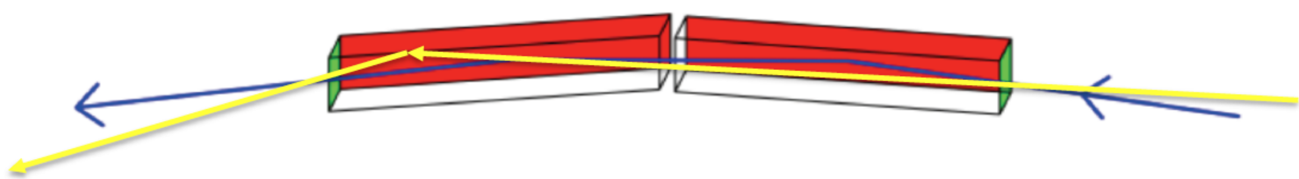

Stray flux – single reflection from 2nd surface in pores

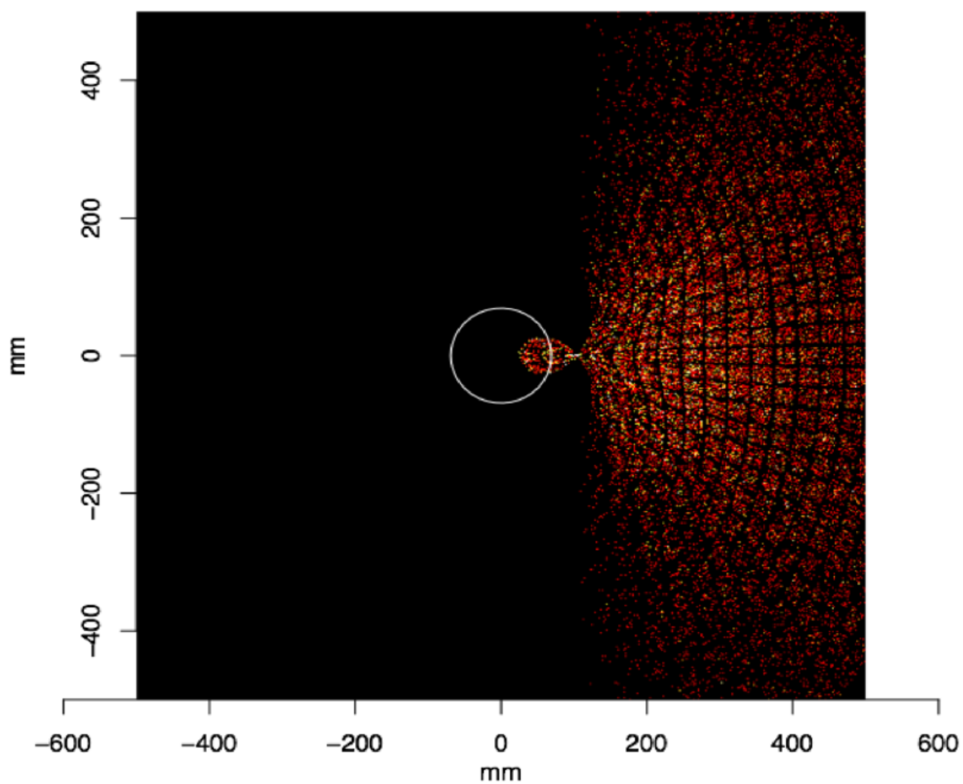

Distribution of flux at 1.25 keV from a point source 30 arc minutes off-axis over the focal plane.

The circle represents the centre of the FOV radius 20 arc minutes.

No baffles or grids on the SPO modules

ATHENA Mirror Assembly – problems

Area vs. energy - imaged and stray

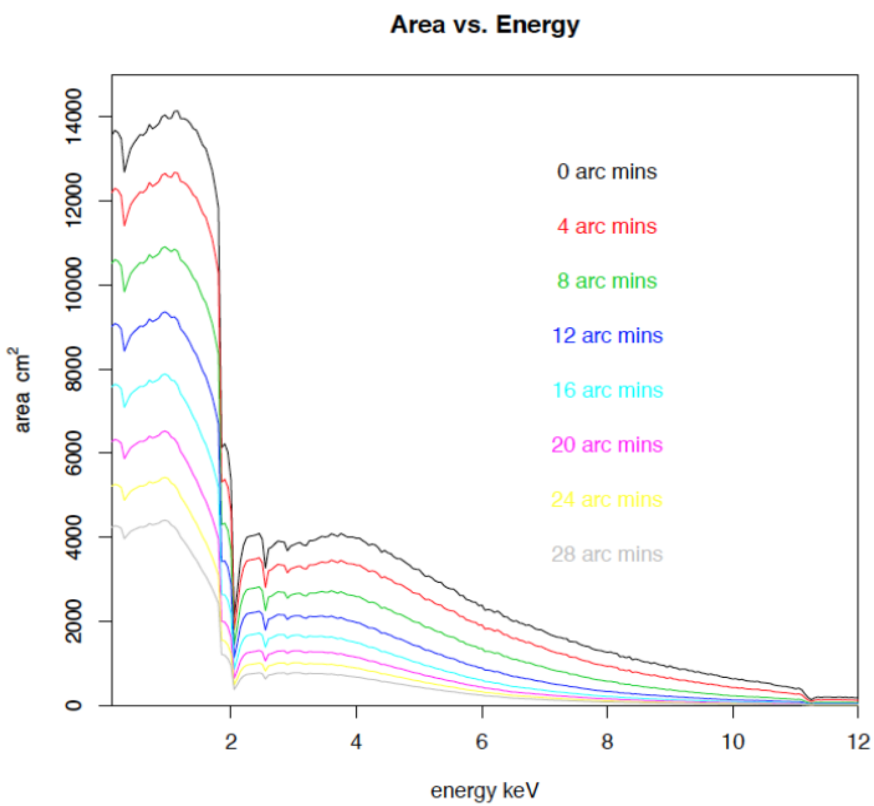

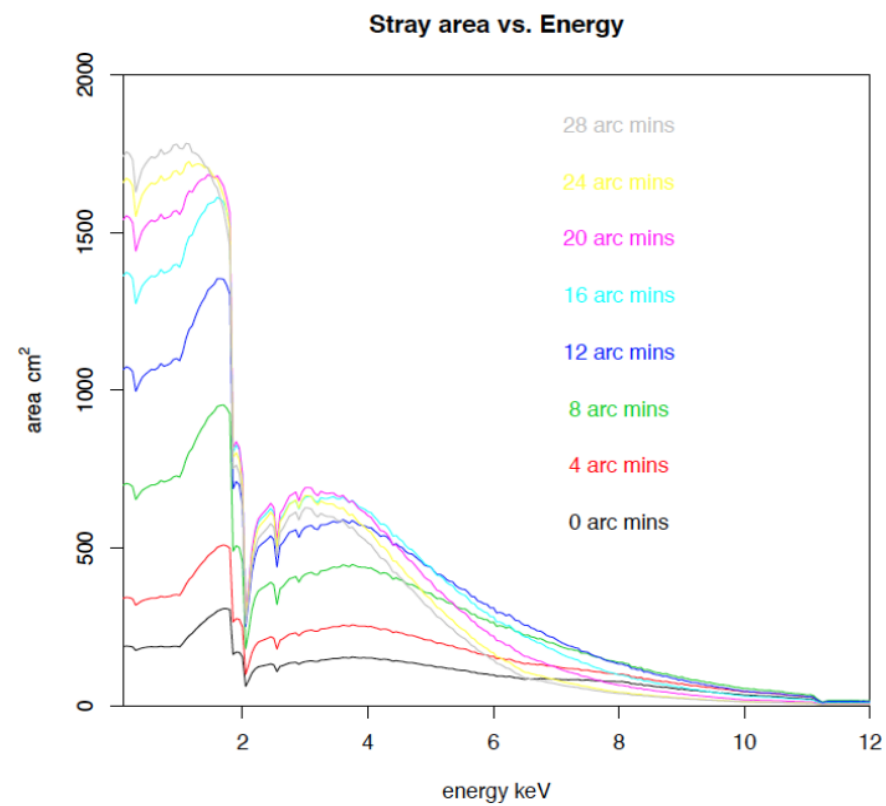

- The stray area corresponds to diffuse flux in the same quadrant but from outside FOV, 18-169 arc mins off-axis
- We can calibrate the stray loading expected - XSPEC ARF for stray

ATHENA Mirror Assembly – new technology Silicon Pore Optic - SPO

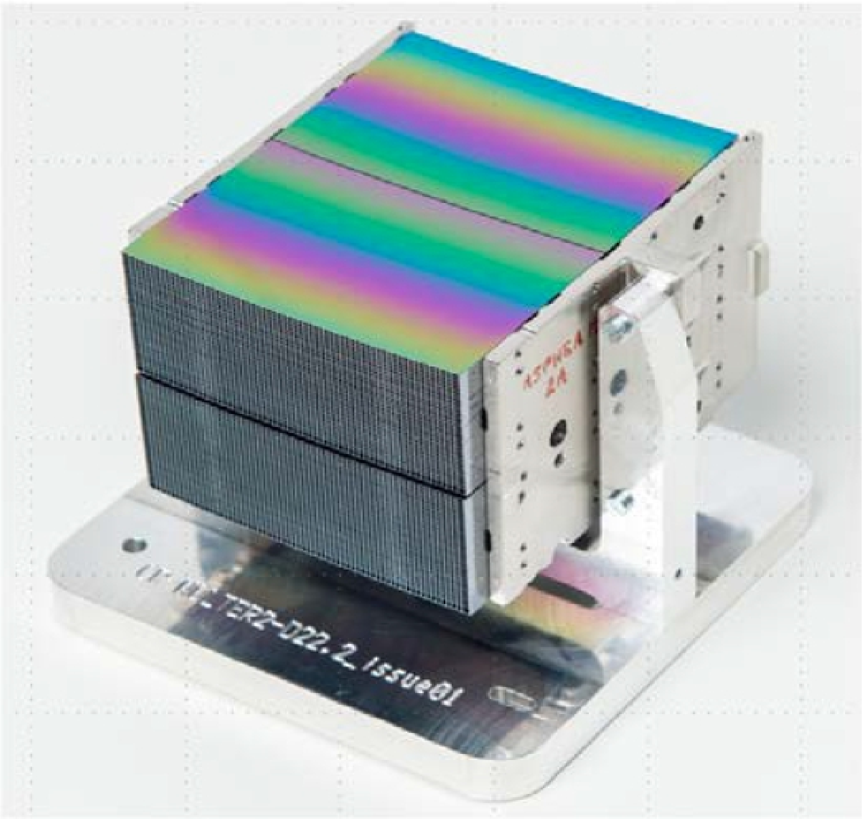

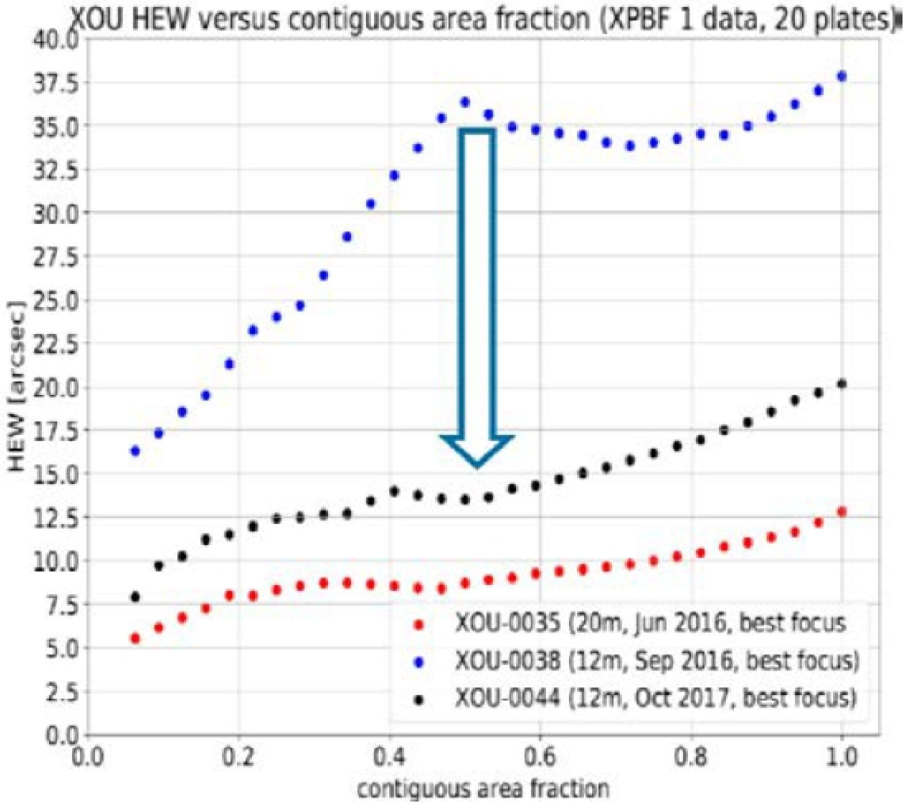

ATHENA Mirror Assembly – new technology
Silicon Pore Optic - SPO

Imaging PSF vs. energy and off-axis angle

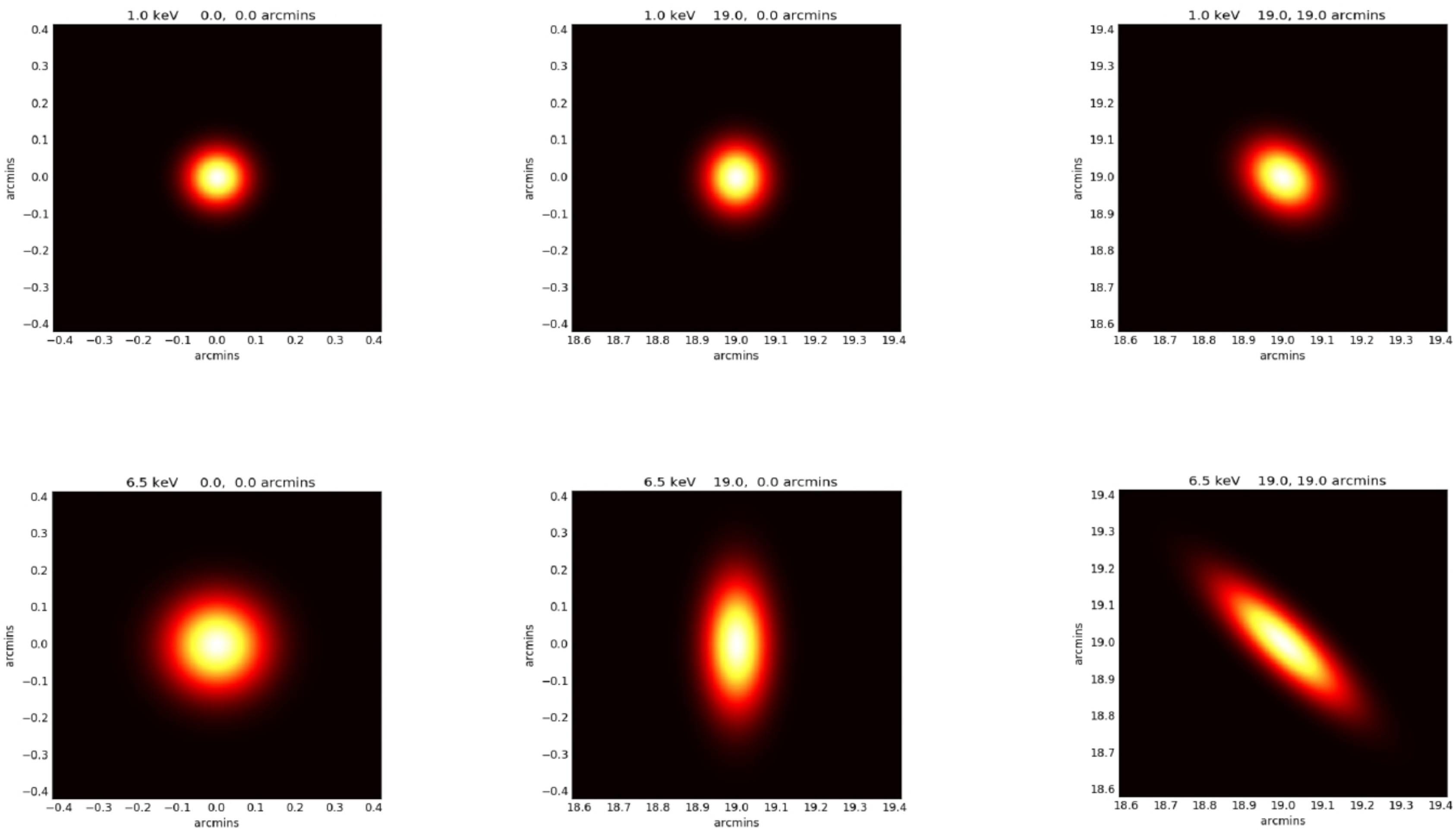

Principles of ranking the lecture:

- to be here

- to participate into discussions

- to make a homework

- hand – on sessions with the use of the computer.....

- to participate in the exam and in exam overview

wi-fi password: a w sercu maj

HEASARC – High Energy Astrophysics Science
Archive Research Center

http://heasarc.gsfc.nasa.gov/

HOMEWORK #2:

Instal HEASoft on the page:
https://heasarc.gsfc.nasa.gov/docs/software/lheasoft/

Up to Nov. 10-17. 2022

send me by e-mail: agata@camk.edu.pl

NEXT LECTURE Nov. 10. 2022

Hands-on session to check HEASoft instalation